Chapter 4

Lattice Design

4.1 Strategy of Lattice Design

The nano-beam scheme[1] is adopted in the lattice design at SuperKEKB. The requirements to accomplish the nano-beam scheme are

1. low emittance in the horizontal and the vertical plane,
2. low beta function at an interaction point in the horizontal and the vertical plane,
3. dynamic aperture to keep enough Touschek lifetime for a top-up injection.

Additional requirements are to reuse magnets of KEKB[2, 3] as much as possible and to fit the beam line to the KEKB tunnel. The parameters related to the lattice design are shown in Table 4.1.

In the case of a low emittance ring, the effect of intra-beam scatterings[4, 5, 6] becomes significantly that affects an emittance, a bunch length, and an energy spread. The vertical emittance is induced by solenoid fringe field, machine errors, and beam-beam effects. However, the vertical emittance should be optimized to achieve the design luminosity. The ratio of the vertical to the horizontal emittance is assumed to be 0.27 % for LER and 0.28 % for HER, respectively. Figure 4.1 and 4.2 show the emittance, the bunch length, and the energy spread as a function of the number of particles per a bunch with keeping the nominal ratio of the vertical emittance.

The lattice design and a tracking simulation of particles are performed by using *SAD*[7] code that has been developed at KEK. The SAD code is a integrated code for an optics matching and a particle tracking that has been successfully used for years at several accelerators such as KEKB and ATF, and so on.

	Symbol	LER	HER	Unit
Energy	E	4.000	7.007	GeV
Beam current	I	3.6	2.6	A
Number of bunches	n_b	2500		
Number of particles per bunch	N	9.04×10^{10}	6.53×10^{10}	
Circumference	C	3016.315		m
Horizontal emittance	ε_x	3.2	4.6	nm
Horizontal beta at IP	β_x^*	32	25	mm
Vertical Beta at IP	β_y^*	270	300	μm
Horizontal betatron tune	ν_x	44.53	45.53	
Vertical betatron tune	ν_y	46.57	43.57	
Synchrotron tune	ν_s	-0.0245	-0.0280	
Bunch length	σ_z	6	5	mm
Momentum compaction	α_p	3.20×10^{-4}	4.55×10^{-4}	
Energy spread	σ_δ	7.92×10^{-4}	6.37×10^{-4}	
Energy loss per turn	U_0	1.76	2.43	MeV
Damping time	$\tau_{x,y}, \tau_s$	45.7, 22.8	58.0, 29.0	msec

Table 4.1: The lattice parameters in LER and HER, respectively. Intra-beam scattering is included in the parameters for the design bunch current.

4.2 Optics Design of Arc Cell

In the case of an electron ring, an equilibrium emittance in the horizontal plane is described by a ratio of a diffusion term due to a quantum excitation to a radiation damping. The emittance can be expressed by radiation integral formulae[8]:

$$\varepsilon_x = \frac{C_\gamma \gamma^2}{J_x} \frac{1}{2\pi\rho^2} \oint H(s) ds, \tag{4.1}$$

where

$$C_\gamma = \frac{55}{32\sqrt{3}} \frac{\hbar}{mc}, \tag{4.2}$$

$$H(s) = \gamma_x \eta_x^2 + 2\alpha_x \eta_x \eta_{p_x} + \beta_x \eta_{p_x}^2, \tag{4.3}$$

J_x is the damping partition number, ρ the curvature of dipole magnets, α_x, β_x, γ_x horizontal Twiss parameters, and η_x, η_{px} horizontal dispersions in the normal coordinate. These formulae are applicable to the case without both X-Y coupling and Z-X coupling. The emittance is calculated by using an envelope method with a 6×6 transfer matrix in general[9]. However, formulae(4.1) is useful to make a track to a low

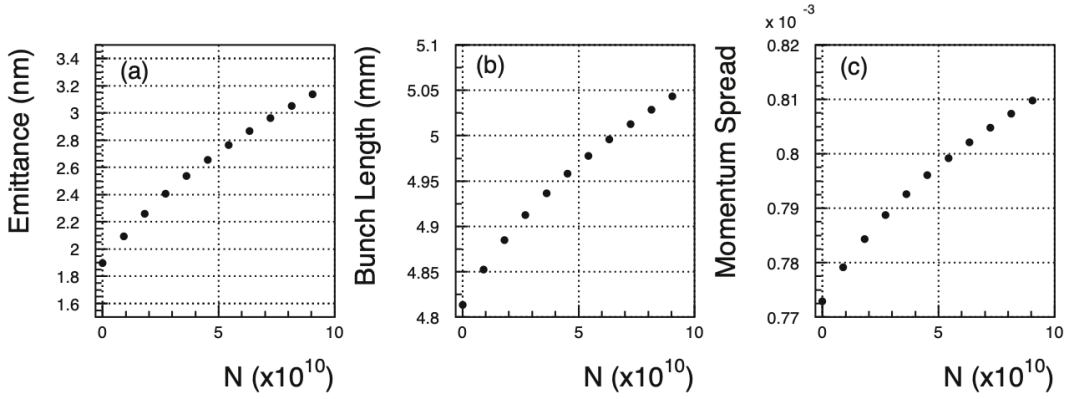

Figure 4.1: Effects of intra-beam scattering in LER. (a) emittance, (b) bunch length, (c) energy spread.

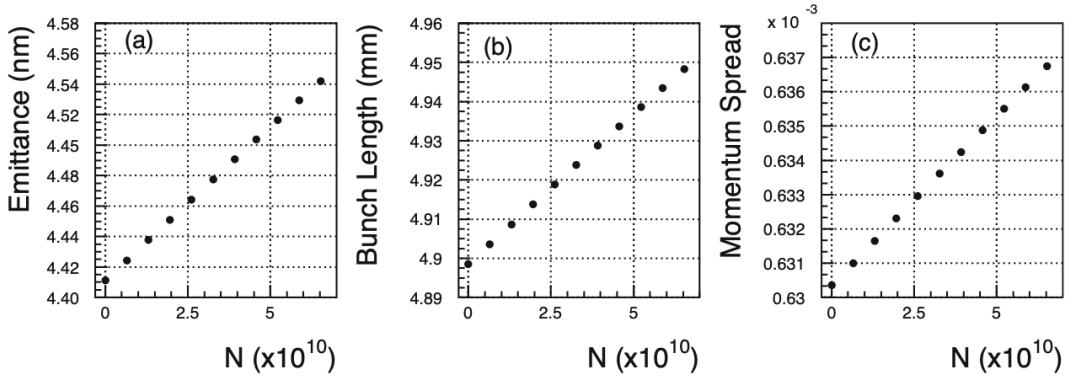

Figure 4.2: Effects of intra-beam scattering in HER. (a) emittance, (b) bunch length, (c) energy spread.

emittance lattice. In order to make the emittance small in the design of an arc cell without neither X-Y coupling nor Z-X coupling, it is necessary to reduce the integration of H in the dipole magnets, to make the curvature of the dipole magnet large, and to make the damping partition number large at the fixed beam energy. It is required that the quadrupole magnets of KEKB are reused as much as possible and the magnet configuration is almost the same as KEKB for the arc cells in SuperKEKB. Therefore, the dipole magnets are replaced by the length of 4.2 m from 0.89 m to make the low emittance in the LER. The beta functions and dispersions are modified to make the emittance as small as possible in the HER as well as the HER. The replacement of the dipole magnets is not planned in the HER because the length of the dipole magnet in KEKB is 5.9 m and already enough long. The beam energy that is changed from 8 GeV to 7 GeV decreases the emittance in the HER. The wiggler section that is described in Sec. 4.4.1 also reduces the emittance in both the LER and the HER. Figures 4.3 and

4.4 show the design of the arc cell in the LER and the HER, respectively.

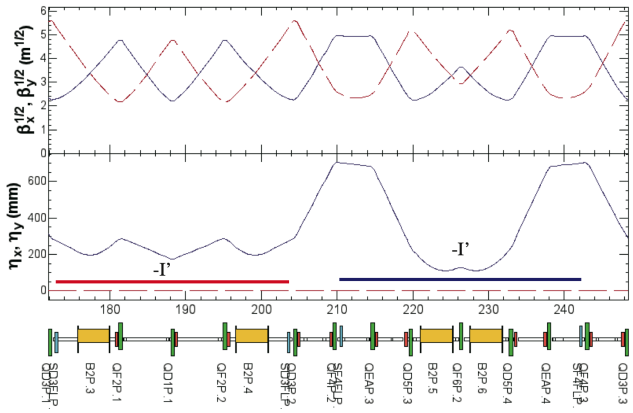

Figure 4.3: Arc cell in LER. Upper indicates beta functions, bottom indicates dispersions.

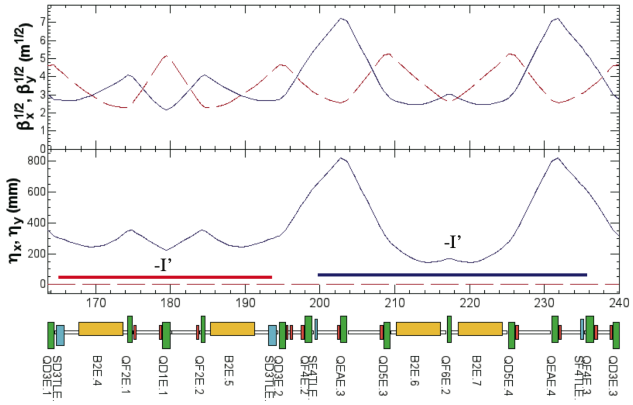

Figure 4.4: Arc cell in HER. Upper indicates beta functions, bottom indicates dispersions.

In SuperKEKB, it is necessary to keep Touschek lifetime as long as possible and to correct a large natural chromaticity. A non-interleaved chromaticity correction is adopted in the arc cell as shown in Figs. 4.3 and 4.4 in order to obtain a large dynamic aperture with a correction of the chromaticity. The transfer matrix between two identical sextupole magnets is $-I'$ to compensate a nonlinear kick due to the strong field of the sextupoles,

$$M_{S_2S_1} = -I' = \begin{pmatrix} -1 & 0 & 0 & 0 \\ m_{21} & -1 & 0 & 0 \\ 0 & 0 & -1 & 0 \\ 0 & 0 & m_{43} & -1 \end{pmatrix}. \tag{4.4}$$

The phase advance between two sextupoles is π in the horizontal and the vertical direction and the configuration of the focusing and defocusing sextupoles are non-interleaved. A nonlinear kick due to one of the sextupole pair can be canceled by the other sextupole magnet for the on-momentum particle, however, the chromaticity can be adjusted properly. The non-interleaved chromaticity correction can be utilized to correct optical functions independently.

The arc lattice is consists of 7 families of quadrupole magnets and 4 dipole magnets in a unit cell. Four families of the quadrupole magnets are used to make a $-I'$ condition and two families can be used to adjust the emittance and the momentum compaction. The variable range of the emittance and the momentum compaction in the arc cell show in Fig. 4.5.

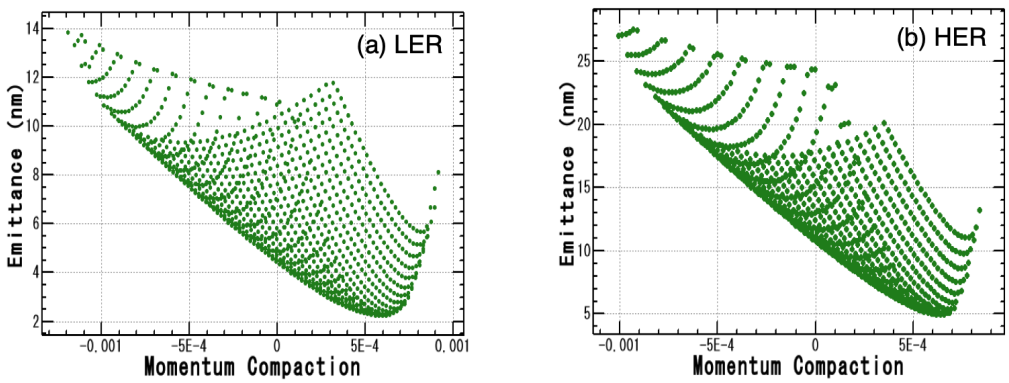

Figure 4.5: Variable range of the emittance and the momentum compaction in the arc cell with the same magnet configuration, (a) LER and (b) HER.

4.3 Optics Design of Interaction Region

4.3.1 Final Focus

The final focus(FF) is designed to achieve extremely low beta at IP. In order to squeeze the beta function, doublets of a vertical focus quadrupole magnet(QC1) and a horizontal focus quadrupole magnet(QC2) are adopted. The QC1 magnets are near IP than QC2 magnets which are independent magnets for each ring. The magnet system consists of superconducting magnets. Since a trajectory of a reference particle is almost passing through the center of the magnet, beam backgrounds of synchrotron

radiation due to the curvature of the trajectory can be reduced which degrades the performance of the Belle II detector. At KEKB, a shared quadrupole magnet was used and trajectories in the LER and in the HER were separated by a kick induced for an off-centered trajectory in the quadrupole magnet at the downstream of IP. On the other hand, it is necessary to make the crossing angle of 83 mrad at SuperKEKB because the trajectories in the LER and in the HER are separated at dipole magnets following the solenoid region.

The final focus magnets have correction coils of a dipole, a skew dipole, a skew quadrupole, a skew sextupole, and/or a octupole field. The final focus magnets except for QC1LP and QC1RP in the LER have an iron or a permendur shield to suppress a leakage field to an opposite beam line. The QC1LP and QC1RP magnets are designed to be an air-core coil because there is a solenoid field of 2 T at the region of the magnets. Therefore, the leakage field from the QC1LP and QC1RP magnets affect the optics in the HER. The leakage field that comes from the LER has no symmetric structure and can become an all ordered multipole field. In order to compensate the sextupole, octupole, decapole, and dodecapole filed while the dipole and quadrupole field are used to adjust optical functions, cancel coils are adopted in the HER. Therefore, the focusing field is included in the optics matching and the leakage dipole field from QC1LP and QC1RP affects the orbit in the HER. The QC1s and QC2s in the HER are shifted parallel to the nominal beam axis by 700 μm in horizontally to make the strength of the dipole field of corrector coils in QC1LE and QC1RE in the HER as small as possible. The angle of the dipole corrector in QC1s is about 1.26 mrad in the HER. Table 4.2 shows the parameters of the final focus quadrupoles.

A solenoid magnet of 1.5 T field is installed in the interaction region(IR) to measure momentum of charged particles generated by physics process. The solenoid magnet is a specific device for colliders and anti-solenoid magnets are adopted to compensate the detector solenoid field. The anti-solenoid magnets are almost overlaid with QC1s and QC2s. Since the axis of the solenoid field and the axis of the beam line are not parallel each other, the fringe field of the solenoid field induces the vertical emittance. The skew dipole field from the fringe is expressed by

$$B_x(s) \simeq -\frac{x}{2}B'_z(s) = -\frac{s\phi_x}{2}B'_z(s), \tag{4.5}$$

where ϕ_x is 41.5 mrad, the half-crossing angle in SuperKEKB. The skew dipole correctors in QC1s and QC2s are used to adjust the vertical orbit to connect the outer region of the solenoid field smoothly on the plane. The vertical emittance depends on the derivative of the B_z and the angle between the axis of the solenoid field and the axis of the beam line. In order to reduce the vertical emittance, the derivative of B_z

	distance from IP(m)	L(mm)	B'(T/m)	Δx(mm)	Δy(mm)	θ(mrad)
QC2LP	1.925	413.5	27.86	0	1.5	-3.725
QC1LP	0.935	337.2	67.94	0	1.5	-13.65
QC1RP	0.930	337.2	66.52	0	1.0	7.204
QC2RP	1.920	413.5	27.76	0	1.0	-2.114
QC2LE	2.700	540.7	26.13	0.7	0	0
QC1LE	1.410	377.4	68.97	0.7	0	0
QC1RE	1.410	377.4	69.48	-0.7	0	0
QC2RE	2.925	422.1	30.59	-0.7	0	0

Table 4.2: Parameters of the final focus quadrupoles at the nominal beam energy. The sign of + indicates outer of the ring in the horizontal direction(x) and downside in the vertical direction(y). The θ shows the rotation angle around the beam axis. The sign of the angle is determined by $-(\vec{e}_x \times \vec{e}_y)$.

should be reduced as much as possible.

Because of about 2 T of the solenoid field at QC1P in the LER, the orbit is curved in the vertical direction. The magnets, QC1LP and QC2LP are moved downside by 1.5 mm and 1.0 mm for QC1RP and QC2RP in the vertical direction in order to reduce the dipole angle of the corrector coil to adjust the orbit as small as possible.

The anti-solenoid magnets are adjusted to fully compensate the detector solenoid for each side of IP as the following:

$$\int_{IP}^{L} B_z(s)ds = 0, \tag{4.6}$$

where L is the distance from IP of 4 m along the beam line that is the solenoid region. The rotation of the final focus magnets around the beam axis and the skew quadrupole correctors are adopted to make vertical dispersions and X-Y couplings in IR as small as possible. For instance, the rotation angle of QC1s and QC2s around the beam axis can be optimized by

$$\theta_{QC} = \frac{1}{2B\rho}\int_{IP}^{QC} B_z(s)ds. \tag{4.7}$$

In the case of the HER, the rotation angles are chosen so as to be zero because θ_{QC} is very small. The skew quadrupole field is corrected by the corrector coils in QC1s and QC2s. The vertical dispersion and the X-Y couplings are corrected in the region prior to a local chromaticity correction. The skew quadrupole magnets outer of the solenoid region are utilized to correct the vertical dispersion and the X-Y couplings in the LER.

In the HER, there are two parts separately, one is the X-Y coupling correction by using skew quadrupole magnets and the other is the vertical dispersion correction by using skew dipole magnets. The vertical emittance from the solenoid fringe after these corrections becomes 0.8 pm for the LER and 1.5 pm for the HER, respectively. These values are much less than the target ratio of the vertical to the horizontal emittance, 0.27(8.64 pm) % in the LER and 0.28 %(12.9 pm) in the HER. Figure 4.6 shows the lattice design of IR in the LER and Fig. 4.7 for the HER. The filed strength of the corrector coils at QC1/QC2 for the nominal beam energy is shown in Table 4.3. The definition of B_n and A_n is written by Eq. (4.10) where L is the effective length.

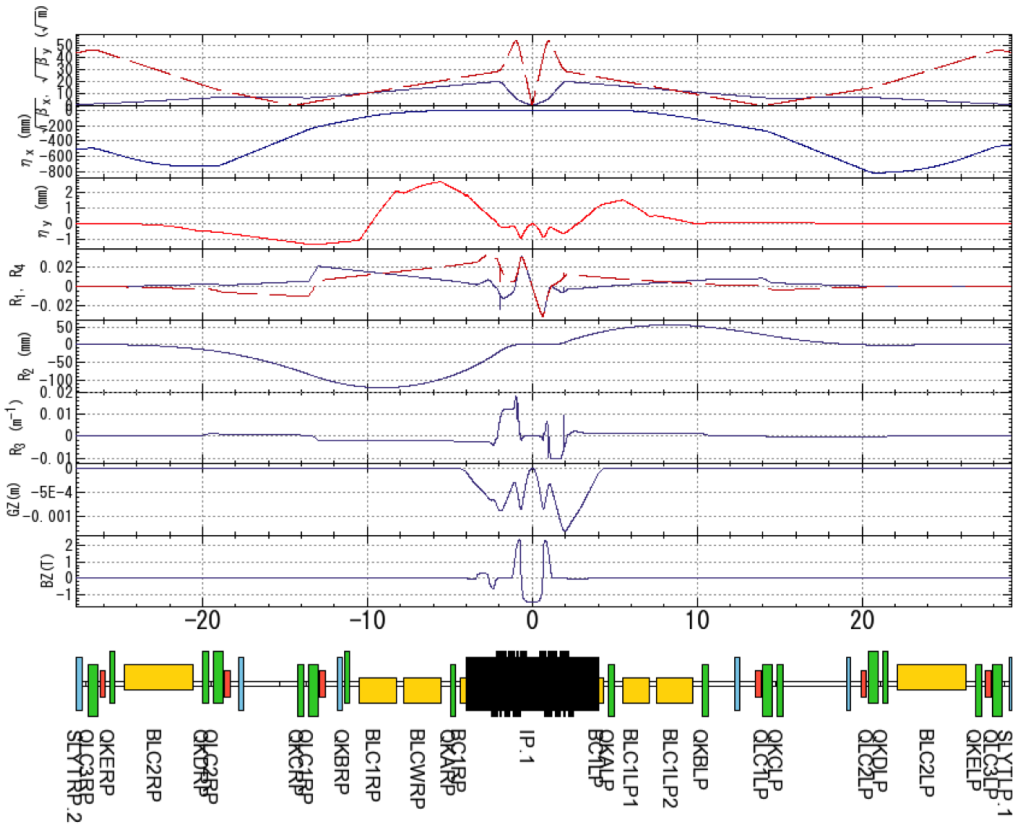

Figure 4.6: Lattice design of the interaction region in the LER.

4.3.2 Local Chromaticity Correction

The natural chromaticity is very large in SuperKEKB as shown in Table 4.4. Since approximately 80 % of the natural chromaticity in the vertical direction is induced in the FF, a local chromaticity correction (LCC) is adopted to correct the large chromaticity near the FF. The LCC consists of two identical sextupole magnets. The transfer ma-

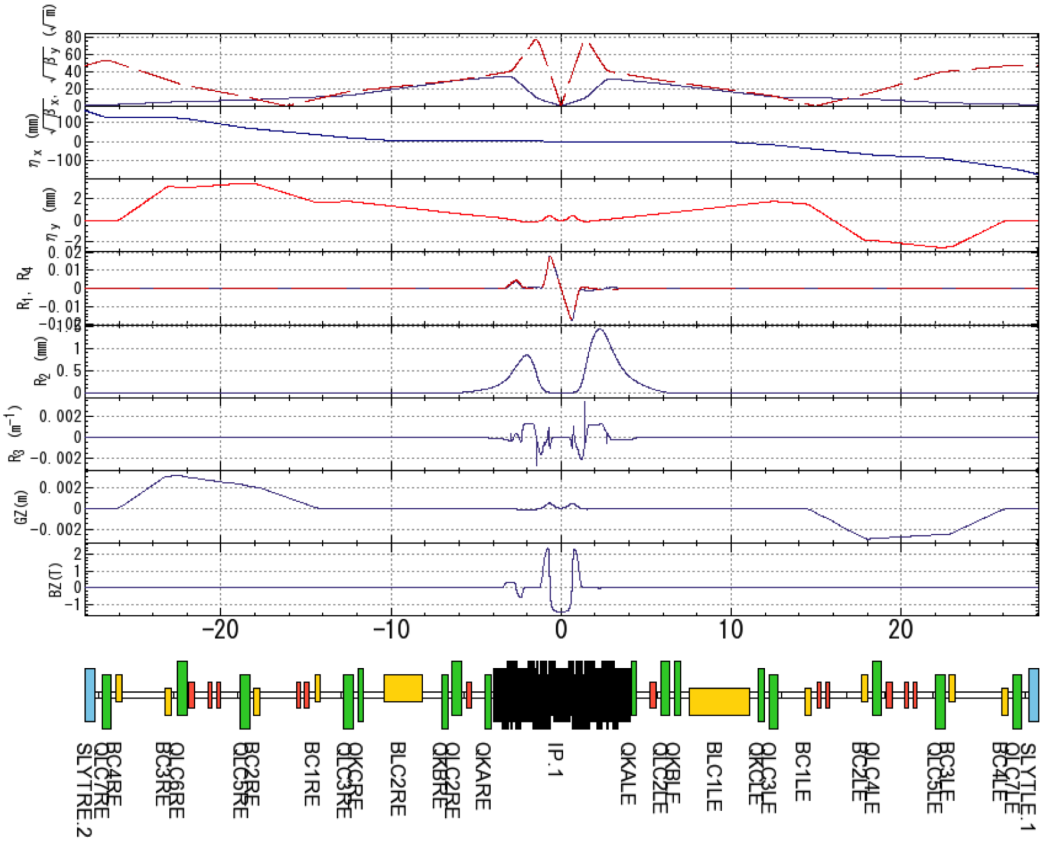

Figure 4.7: Lattice design of the interaction region in the HER.

Location	B_1L(Tm)	A_1L(Tm)	A_2L(Tm)	B_4L(Tm)	r_0(mm)
QC2LP	-0.0217	0.0220	-2.8×10^{-4}	0.0013	30
QC1LP	0.0040	-0.0020	0	-2.7×10^{-5}	10
QC1RP	0.0050	-0.0086	0	-2.7×10^{-5}	10
QC2RP	-0.0228	0.0214	0	N/A	30
QC2LE	0	-0.0164	9.48×10^{-4}	9.75×10^{-4}	35
QC1LE	0.0301	0.0092	-0.00109	3.64×10^{-5}	15
QC1RE	-0.0305	0.0053	9.79×10^{-4}	N/A	15
QC2RE	0	-0.0022	0.00196	N/A	35

Table 4.3: Parameters of the corrector coils at the nominal beam energy. The octupole coils are necessary to make the dynamic aperture large.

trix between two sextupoles is $-I'$ to compensate a nonlinear kick due to the strong field of the sextupoles as the same as that of the arc section. Both the horizontal and the vertical LCCs are considered in SuperKEKB. There are four families of sextupole magnets, one is the vertical (Y-LCC) and the other is for the horizontal chromaticity correction (X-LCC). The phase advance QC1 and the Y-LCC is π in the vertical direction and between QC2 and the X-LCC is 2π in the horizontal direction for each side of IP. Horizontal dispersions are made at the LCC by using several dipole magnets. Figure 4.8 shows the lattice design of the LCC region in the LER and that of the HER is shown in Fig. 4.9, respectively.

		SuperKEKB		KEKB	
		LER	HER	LER	HER
Horizontal chromaticity	ξ_{x0}	-105	-171	-72	-70
Vertical chromaticity	ξ_{y0}	-776	-1080	-123	-124

Table 4.4: Comparison of natural chromaticity in SuperKEKB with KEKB.

4.4 Optics Design of Straight Section

New wiggler magnets are installed in the LER. The wiggler has a shorter periodic structure than that of KEKB. The location of the wiggler section is NIKKO and OHO. The ARES cavities are located in FUJI(D7 and D8) and in OHO(D5). In the HER, the wiggler is installed in OHO(D5). The wiggler magnets used in the LER at KEKB are

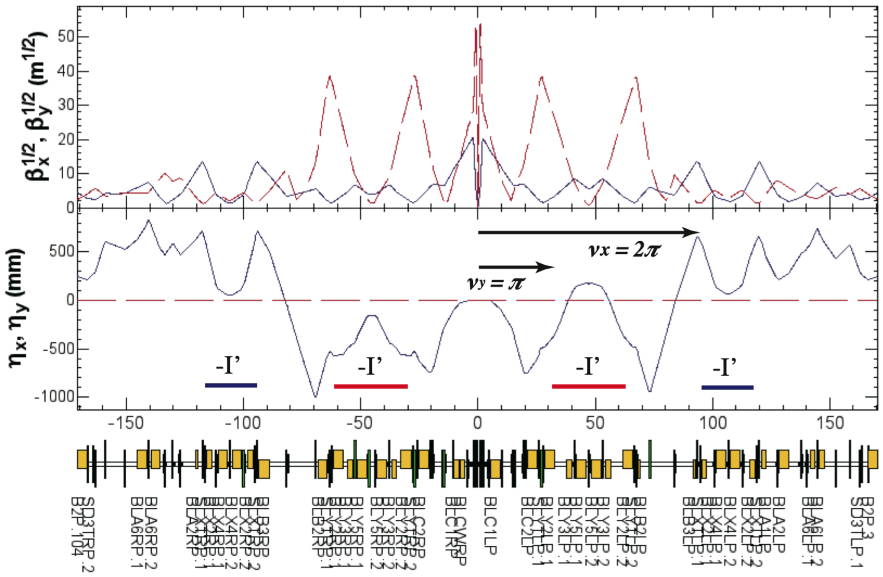

Figure 4.8: IR lattice in the LER. Red bar indicates the vertical LCC and blue bar indicates the horizontal LCC.

reused in the HER. The ARES cavities are located in OHO(D4) and the SCC cavities are located in NIKKO(D10 and D11) in the HER.

4.4.1 Wigglers

Wiggler magnets are installed to each ring to make the emittance small in addition to the modification of the arc lattice. The emittance is modified by

$$\varepsilon_x = \frac{C_\gamma \gamma^2}{J_x} \frac{I_{5,arc} + I_{5,wig.}}{I_{2,arc} + I_{2,wig.}}, \tag{4.8}$$

where the suffix of *arc* and *wig.* indicates the region of the integration. In the case of the LER, the emittance becomes 1.87 nm with the wiggler section although the emittance of the arc cell is 4.08 nm. The wiggler section in the LER is shown in Fig. 4.10 and that of the HER in Fig. 4.11, respectively. The wiggler section can be used to make a high emittance lattice up to 20 nm by using only the NIKKO straight section(No rf cavity). The high emittance lattice makes Touschek lifetime longer and can perform in a vacuum scrubbing. Table 4.5 shows the lattice parameters when the wiggler magnets are turned off.

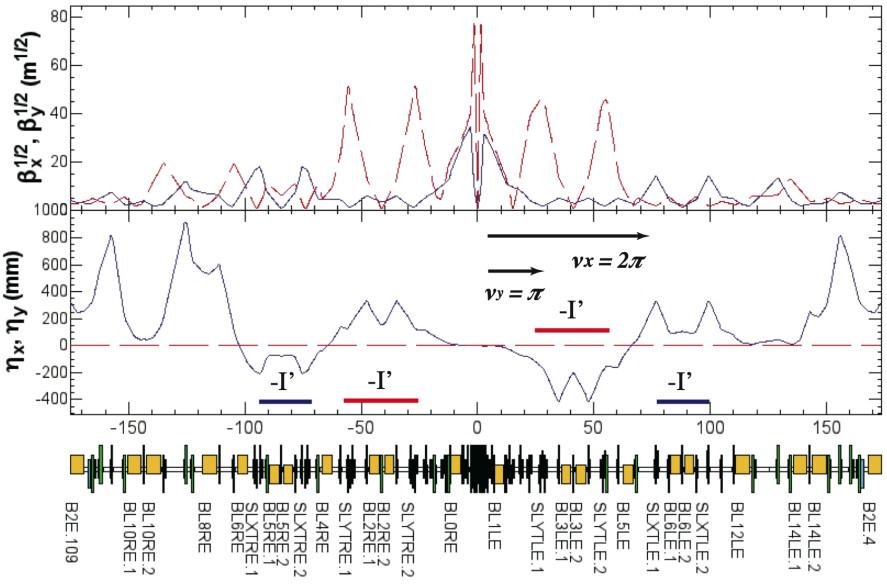

Figure 4.9: IR lattice in the HER. Red bar indicates the vertical LCC and blue bar indicates the horizontal LCC.

	Symbol	LER	HER	Unit
Emittance	ε_x	6.20	5.11	nm
Horizontal damping time	τ_x	213	68	msec
Change of circumference	Δz	-6.32	-0.394	mm

Table 4.5: The lattice parameters without wigglers in LER and HER, respectively. Intra-beam scattering is not included in the parameters.

4.4.2 Chicane

The circumference is adjusted by using a frequency of a rf system in the HER. Since the rf frequency is a common in the HER and the LER, the circumference of the LER is adjusted by another way such as a chicane independently. The chicane is located in the upper stream of the NIKKO (D11) straight section in the LER. The chicane consists of four dipole magnets. The variable range of the circumference is ±3 mm. The maximum bending angle is 38.83 mrad for each dipole magnet and the nominal angle is 27.46 mrad for the middle of the range. In order to settle the same circumference between the LER and the HER, the beam lines should be aligned so as to be less than ±3 mm for the discrepancy.

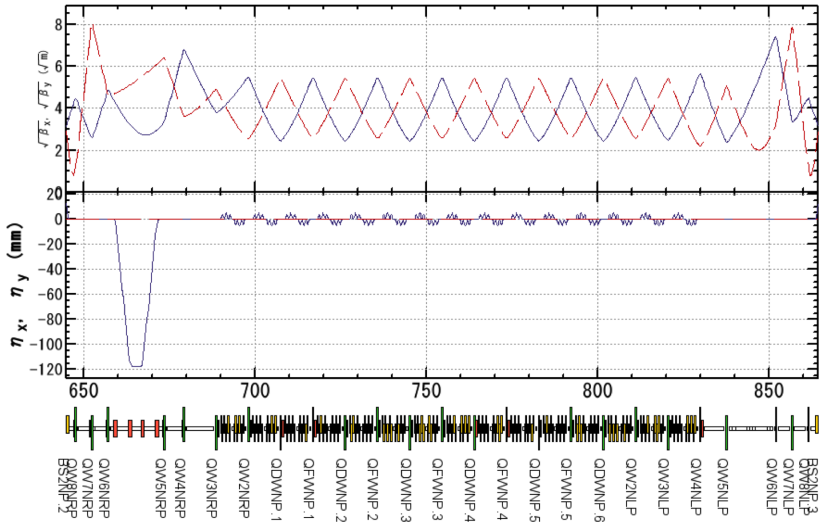

Figure 4.10: Wiggler section in LER(NIKKO).

4.4.3 Injection and Abort System

Injection and abort system are located in the FUJI straight section. The beam injection is a multi-turn injection, two injection kickers make a local bump orbit for a storage beam so as to merge a injected beam. The horizontal phase advance between two injection kickers is π. The nominal horizontal beta function at the injection point is 100 m in the case of betatron phase space injection. The injection in a synchrotron phase space is also considered in the HER due to lack of enough transverse aperture. The abort system utilizes abort kickers and two sextupole magnets to increase beam size at the abort window in the HER. The two sextupole magnets are located at dispersion free and are connected by $-I'$ to cancel a nonlinear kick by themselves. The strength of the sextupole magnets is determined by a requirement of the abort system. The abort system in the LER utilizes abort kickers and pulse quadrupole magnets to make a beam size large at the abort window. The magnet configuration in the details can be found in this report.

4.5 Dynamic Aperture

The dynamic aperture is restricted due to nonlinear effects in the optics. The nonlinear effect in the final focus system decreases the dynamic aperture significantly. The nonlinear effect becomes large since the magnetic field reaches 70 T/m for the main field with higher order multipole fields and the beta function at the magnet is much larger than the other sections. In addition to the nonlinear magnetic field, the drift space is

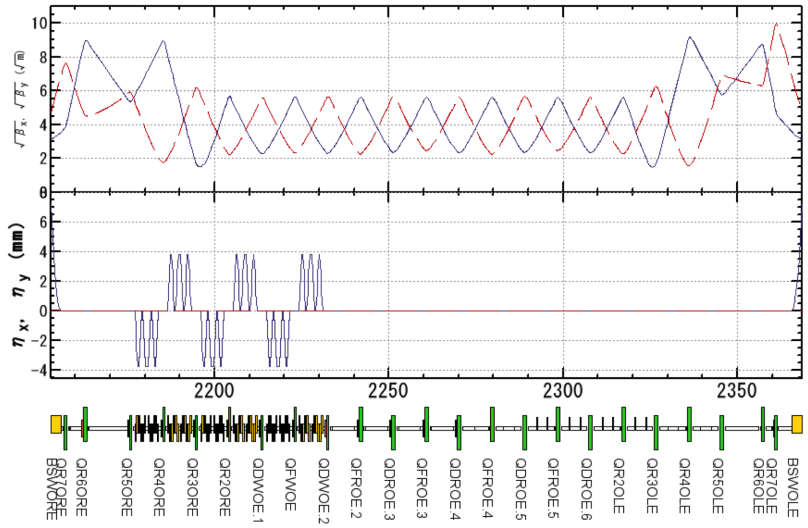

Figure 4.11: Wiggler section in HER(OHO).

not liner system as shown in the Hamiltonian. Especially, when the beta function is squeezed in the vicinity of IP and decreased with distance from IP, the effect cannot be ignored. The Hamiltonian for the nonlinear effects such as kinematic terms and nonlinear Maxwellian fringe effects is written by[10]

$$H_{nl} = \left(1 - \frac{2}{3}k_1 L^{*2}\right) \frac{L^*}{\beta_y^{*2}} J_y^2 \cos\psi_y^4, \tag{4.9}$$

where $k_1 = B'/B\rho$ is the strength of the magnetic field, L^* is the distance from IP to the final focus magnet. Table 4.6 shows the coefficient of the Hamiltonian to evaluate the dynamic aperture in SuperKEKB. The fringe field in the FF is very strong compared with that of KEKB. Therefore, the dynamic aperture will be restricted by the fringe field near IP significantly.

			β_y^* (μm)	k_1 (1/m^2)	L^* (m)	coefficient (1/μm)
SuperKEKB	LER	L-side	270	-5.104	0.766	31.55
		R-side		-5.104	0.761	31.06
	HER	L-side	300	-3.0539	1.221	54.64
		R-side		-2.878	1.221	52.36
KEKB		L-side	5900	-1.777	1.332	0.119
		R-side		-1.778	1.762	0.237

Table 4.6: Dynamic aperture is restricted by nonlinear effects.

It is difficult to apply either an analytic approach or a perturbative method to an

evaluation of the dynamic aperture since there is the final focus system as described above and the sextupole magnets to correct the large chromaticity causes strong nonlinear effects. Therefore, the dynamic aperture is estimated by using SAD. Six canonical variables, x, p_x, y, p_y, z, and δ are used to describe the motion of a particle, while p_x and p_y are transverse canonical momenta normalized by the design momentum, p_0, and δ is the relative momentum deviation from p_0. A synchrotron oscillation is included while a synchrotron radiation and a quantum excitation are turned off during tracking simulations. The FF region within $\pm$ 4 m from IP, the magnetic field of Belle II and the anti-solenoids and QCS(QC1 and QC2) along the longitudinal direction on the beam line is sliced by thickness of 10 mm of constant B_z or $K_1 = B'L/B\rho$ to make the lattice model. Higher order multipole fields up to 44-poles for normal and skew fields are included in the slices[11]. The three-dimensional solenoid field is calculated by using ANSYS[12] which is a electromagnetic field simulation code. The behavior of the solenoid field is also implemented by slices in the model[13]. The fringe field of the solenoid field and higher order multipole fields of the final focus magnets affect the dynamic aperture significantly.

The arcs of the SuperKEKB rings consist of 2.5π unit cells that include non-interleaved sextupole pairs for chromaticity corrections. Two non-interleaved sextupole magnets are placed in a cell, and the number of the sextupole pairs in the whole ring amounts to 50. The local chromaticity corrections similar to the arc cell are also placed in the TSUKUBA straight section to correct large chromaticity induced by the FF. Two sextupole magnets in a pair are connected with a $-I'$ transformer. By this arrangement, the principle nonlinearities of the sextupoles are canceled in each pair, which creates a large transverse dynamic aperture.

The beam lifetime should be long enough to store the beam currents stably. Touschek lifetime contributes the total lifetime significantly because of the low emittance in SuperKEKB. The target of Touschek lifetime is 600 sec for the nominal machine parameters in SuperKEKB. Touschek lifetime depends on the dynamic aperture and the density of particles in a bunch. The larger dynamic aperture is obtained by optimizing 54 families of sextupoles and 12 (LER) or 10 (HER) families of skew sextupoles in both the arc and the LCC, and 3 (LER) or 2 (HER) octupole coils in QCs. The optimization utilizes an off-momentum matching and a down-hill simplex method as a function of an area of the dynamic aperture. The octupole magnets make the transverse dynamic aperture larger by deforming the phase space at the large amplitude to fit the physical aperture. The skew sextupole magnets correct chromatic X-Y coupling. The skew sextupole filed is induced by rotating the normal sextupole in the LER. In the HER, the skew sextupole magnets are placed in the vicinity of the sextupole magnets in the

arc cells.

The dynamic aperture is estimated by a particle tracking in the LER and the HER, respectively. The particle tracking is performed for 1000 turns to define a stable region with synchrotron oscillations. The dynamic aperture is important for keeping enough Touschek lifetime as well as an injection aperture. Figure 4.12 shows the dynamic aperture in the LER and the HER, respectively. The area of the dynamic aperture is fitted by an ellipse to estimate Touschek lifetime. Two initial betatron phase of $(0, 0)$ and $(\pi/2, \pi/2)$ in the horizontal and vertical plane are calculated in the dynamic aperture survey. Touschek lifetime is defined by average of two cases since the larger betatron amplitude becomes a nonlinear region and a Poincare plot differs from a circle. The requirement of Touschek lifetime is almost satisfied in the ideal lattice and the optimization has been still continued. Figure 4.13 shows the dynamic aperture in the betatron tunes in the case that both of the initial vertical amplitude and momentum deviation is zero. The nominal betatron tune is $(\nu_x, \nu_y) = (44.53, 46.57)$ in the LER and $(\nu_x, \nu_y) = (45.53, 43.57)$ in the HER, respectively.

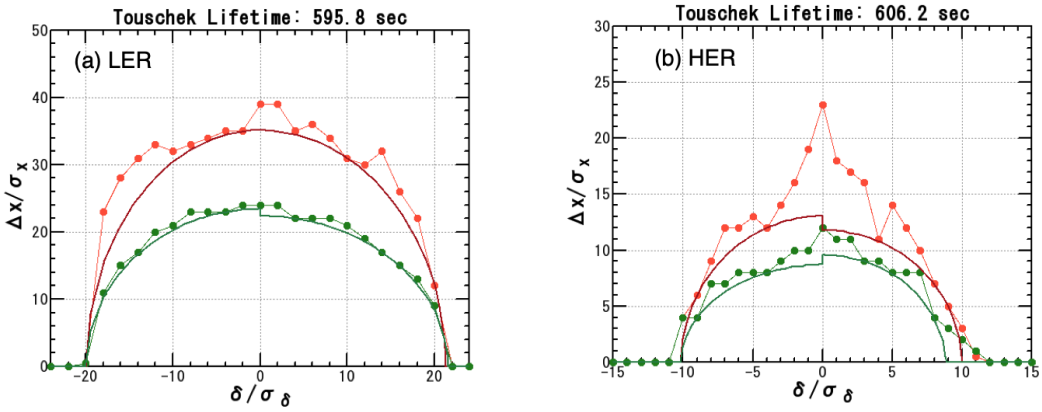

Figure 4.12: Dynamic aperture. (a) LER, (b) HER. Touschek lifetime is estimated by the dynamic aperture. Red line indicates $(\psi_{x0}, \psi_{y0}) = (0, 0)$ for the initial phase and green line indicates that the initial phase is $(\psi_{x0}, \psi_{y0}) = (\pi/2, \pi/2)$.

4.6 Machine Error and Optics Correction

4.6.1 Tunnel Subsidence and Alignment Strategy of Magnet

Main rings, LER and HER at SuperKEKB are constructed in the same tunnel of KEKB. The beam line is almost reused except for the TSUKUBA region. The level markers of the tunnel have been measured since 1998[14] and a subsidence of the

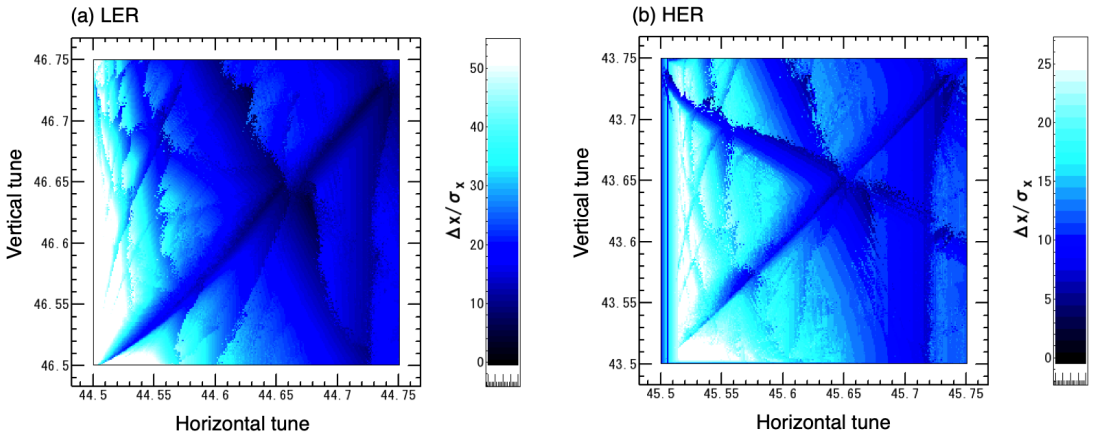

Figure 4.13: Dynamic aperture in the plane of betatron tunes without an initial vertical amplitude and momentum deviation. (a) LER, (b) HER.

tunnel has occurred year by year. The subsidence is not uniform along the beam line. The variation of the level marker in the vertical direction is shown in Fig. 4.14. The reference point is a level marker in the vicinity of IP. The maximum subsidence of the tunnel reaches about 28 mm at $s = 1900$ m. The fastest speed of the subsidence is about 2 mm/year in the whole ring.

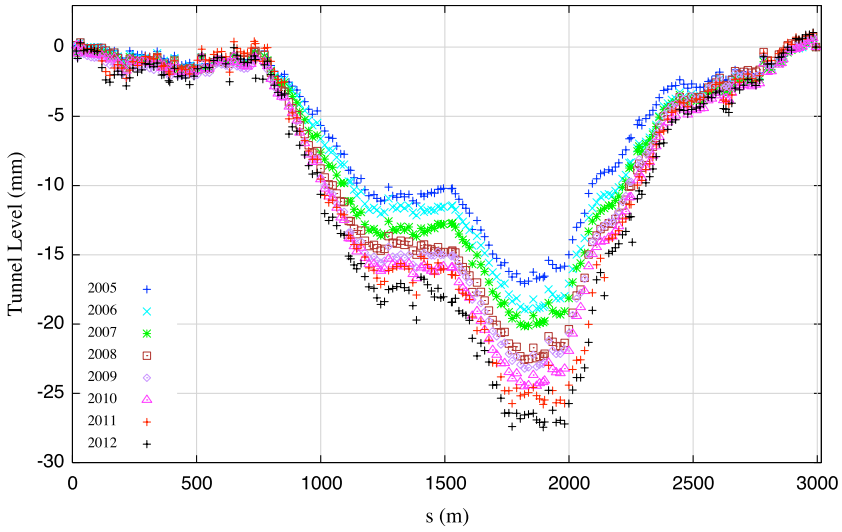

Figure 4.14: Subsidence along the beam line year by year. The reference point is $s = 0$ at IP.

The vertical emittance is restricted by the variation of the beam line that is shorter periodic length than the distance among dipole correctors and skew quadrupole magnets to correct closed orbit distortions and X-Y couplings. Another is a faster variation of the beam line than a interval of optics corrections. The level of the tunnel was zero

at the beginning of the KEKB experiment. When the level of the beam line is corrected to be zero in the vertical direction, the level has to be corrected by about 28 mm at the maximum. However, it is difficult for the rf cavities to make an alignment procedure due to a lack of the range of the vertical adjustment. There is another way to make a plane that includes midpoints of three rf straight sections. In this case, the maximum adjustment of the beam line can be reduced by about 10 mm at the maximum. However, it is found that a smooth beam line from a large perspective satisfies the requirement of the vertical emittance and a luminosity performance from optics simulations. The adjustment becomes less than about 1 mm in this procedure. It is advisable to make the smooth beam line since the workload can be reduced by decreasing the large amount of the adjustment. The strategy of the magnet alignment is:

- a target for the reused beam line is a smooth beam line that is made by a low-pass filter along the beam line (a cut-off wave length is 150 m at least.),
- a horizontal plane that includes IP in the TSUKUBA straight section (new beam line),
- the reused beam line and the new beam line is connected smoothly.

The alignment of the vertical local chromaticity correction (Y-LCC) is very sensitive to the deterioration of the vertical emittance. For instance, a change of room temperature affects the length of supports for the magnets in the Y-LCC region and then the magnets are misaligned. It is necessary to make the accurate alignment procedure and to keep the magnet position stable for the Y-LCC region. The alignment of the final focus system is also sensitive to the vertical emittance. Especially, a vibration of the QC1s and QC2s in the vertical direction deteriorates the vertical emittance. The worst case is an opposite direction of the vibration between the left side and the right side of IP. The increase of the vertical emittance is ignored when the vertical amplitude of the vibration is less than 200 nm for the QC1s and QC2s.

If a subsidence occurs locally and the vertical emittance deteriorates, the alignment procedure of the beam line is adopted again during a long-term shutdown at the SuperKEKB experiment.

4.6.2 Requirements on Magnet System

The tolerance of the systematic multipole field of the dipole and quadrupole magnets is required to be the same as that of KEKB. The dynamic aperture is almost restricted

by the nonlinear field of the final focus magnets. The expansion of the magnetic field is defined by[1]

$$B_y + iB_x = \sum_{n=1}^{\infty}(B_n + iA_n)\left(\frac{x+iy}{r_0}\right)^{n-1}, \tag{4.10}$$

where r_0 is the reference radius. Table 4.7 shows the requirements of the multipole error in the arc section. The magnets have to be compact since the space near the solenoid region is very tight. The tolerance of the magnets near the solenoid region is shown in Table 4.8.

	B_3/B_1 (%)	B_5/B_1 (%)	r_0 (mm)
Main dipole	0.12	0.45	50
	B_6/B_2 (%)	B_{12}/B_2 (%)	r_0 (mm)
Quadrupole	0.12	0.14	50

Table 4.7: Tolerance of systematic multipole field error in the arc section. The reference radius is 50 mm.

Since the FF system is very sensitive to the ring lattice, the change of magnetic field on the beam line affects both of the beam orbit in the vicinity of IP and the vertical emittance. The requirements are

- the vertical beam orbit, $\Delta y/\sigma_y^* < 0.1$,
- the vertical emittance, $\varepsilon_y/\varepsilon_y(0) < 0.1$, where $\varepsilon_y(0)$ is the nominal value.

The field ripple larger than 50 Hz will become a serious matter to make an optimization of the luminosity. The filed ripple for the main coils and A1 corrector coils are required to be less than 10 ppm(peak-to-peak field) along the beam line. The requirement of the ripple of power supplies relaxes because of the shield effect of the vacuum chamber between the magnet and the beam line. The eddy currents in the vacuum chamber should be considered. If the phase of the field ripple can be 180 degree between the left-side and right-side of IP, the field ripple will be almost compensated or reduced by 1/2∼1/3 since the betatron phase advance is π between them.

4.6.3 Optics Correction

The most important issue is a reduction of the vertical emittance induced by machine error because it is necessary for the vertical emittance to be as small as possible to

[1]European convention

	L (m)	B_3/B_1 (%)	r_0 (mm)
BLC1LP1,	1.59	1	50
BLC1LP2, BLC1RP, BLCWRP	2.23	1	
	L (m)	B_3/B_1 (%)	r_0 (mm)
BC1LP, BC1RP	0.3444	3	
BLC1LE	3.6	1	
BLC2RE	2.23	1	40
BC1LE-BC4LE	0.3444	3	
BC1RE-BC4RE	0.3444	3	
	L (m)	B_6/B_2 (%)	r_0 (mm)
QLC2LE, QLC2RE	0.56	0.5	40

Table 4.8: Tolerance of systematic multipole field error for dipoles and quadrupoles near solenoid region. The L indicates effective length of magnets.

achieve the target luminosity. Misalignment and field gradient error of the magnets are assumed as the machine error. The rotation error of the quadrupole magnets around the beam axis and the vertical displacement of the sextupole magnets increase the vertical emittance. Figure 4.15 shows the vertical emittance as a function of the rotation angle of the quadrupole magnets except for the final focus system. Figure 4.16 shows the vertical emittance as a function of the vertical displacement of the sextupole magnets in the arc section. The rotation error is assumed to be 100 μrad as an average value of about 450 quadrupole magnets for each ring. On the other hand, the vertical displacement is assumed to be 100 μm as an average value of 100 sextupole magnets. It is found that the vertical emittance becomes lager than 10 pm without any optics corrections in the realistic case.

There are two methods to measure a X-Y coupling that induces a vertical emittance. One is a measurement based on a response of closed orbit distortion (COD) and the other is a phase space analysis of second-order moment by using single-pass BPMs. The number of BPMs is 444 in the LER and 466 in the HER. The number of the single-pass BPMs is 135 out of averaged-mode BPMs for each ring. Skew quadrupole coils at sextupole magnets are utilized to correct measured X-Y couplings. In an X-Y decoupled coordinate system, the canonical variables of a particle can be described as

$$\begin{pmatrix} u \\ p_u \\ v \\ p_v \end{pmatrix} = \begin{pmatrix} \mu & 0 & -r_4 & r_2 \\ 0 & \mu & r_3 & -r_1 \\ r_1 & r_2 & \mu & 0 \\ r_3 & r_4 & 0 & \mu \end{pmatrix} \left\{ \begin{pmatrix} x \\ p_x \\ y \\ p_y \end{pmatrix} - \begin{pmatrix} \eta_x \\ \eta_{px} \\ \eta_y \\ \eta_{py} \end{pmatrix} \delta \right\} \tag{4.11}$$

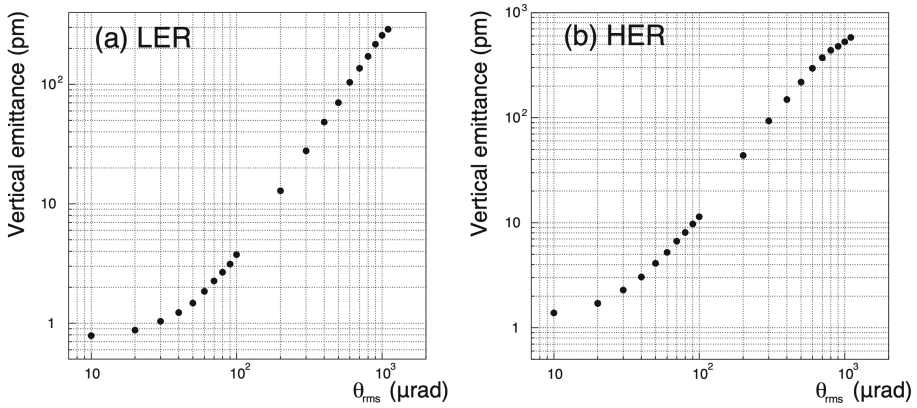

Figure 4.15: Vertical emittance as a function of rotation error of quadrupoles except for the final focus quadrupoles. The vertical emittance is an average value obtained from simulations of 1000 samples. (a) LER, (b) HER.

and the normal dispersions are given by

$$\begin{pmatrix} \eta_u \\ \eta_{pu} \\ \eta_v \\ \eta_{pv} \end{pmatrix} = \begin{pmatrix} \mu & 0 & -r_4 & r_2 \\ 0 & \mu & r_3 & -r_1 \\ r_1 & r_2 & \mu & 0 \\ r_3 & r_4 & 0 & \mu \end{pmatrix} \begin{pmatrix} \eta_x \\ \eta_{px} \\ \eta_y \\ \eta_{py} \end{pmatrix}, \tag{4.12}$$

where

$$\mu^2 + (r_1 r_4 - r_2 r_3) = 1, \tag{4.13}$$

(x, p_x, y, p_y) are the physical orbits and $(\eta_x, \eta_{px}, \eta_y, \eta_{py})$ are physical dispersions in a laboratory coordinate system. We refer to (r_1, r_2, r_3, r_4) as X-Y coupling parameters. The leakage vertical orbits induced by horizontal dipole correctors have been observed by averaged-mode BPMs and corrected to be the model response by using local bump orbits at the sextupole magnets during KEKB operation. The measurement method can be also applicable to SuperKEKB. On the other hand, the X-Y coupling can be measured by using single-pass BPMs where the bunch is kicked by a kicker[15]. A betatron oscillation of a *pilot bunch* measured by the single-pass BPMs is a feasible approach to obtain optical functions during beam collisions at a high current. The pilot bunch is a non-collision bunch located at the tail of a bunch train. In the case of a bunch kicked in the horizontal direction (H-mode), the relation between the physical variables and the X-Y coupling parameters can be expressed by

$$\begin{pmatrix} r_1 \\ r_2 \\ r_3 \\ r_4 \end{pmatrix} = -\mu \Sigma^{-1} \begin{pmatrix} < xy > \\ < xp_x > \\ < xp_y > \\ < p_x p_y > \end{pmatrix}, \tag{4.14}$$

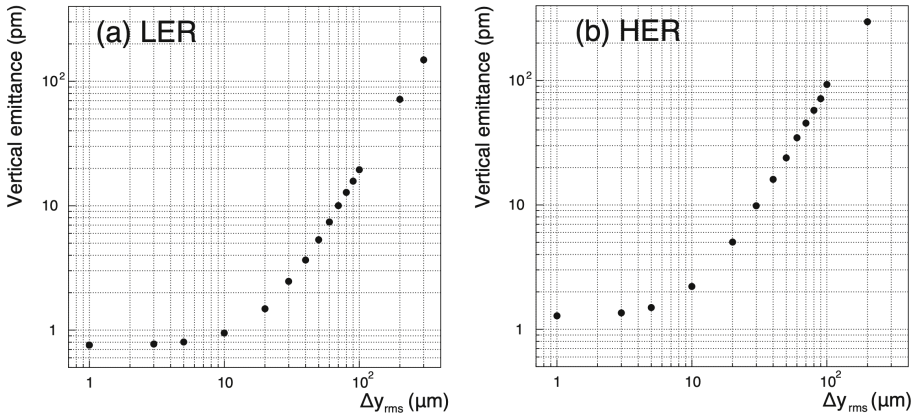

Figure 4.16: Vertical emittance as a function of vertical displacement of sextupoles in the arc section. The vertical emittance is an average value obtained from simulations of 1000 samples. (a) LER, (b) HER.

where

$$\Sigma = \begin{pmatrix} < x^2 > & < xp_x > & 0 & 0 \\ < xp_x > & < p_x^2 > & 0 & 0 \\ 0 & 0 & < x^2 > & < xp_x > \\ 0 & 0 & < xp_x > & < p_x^2 > \end{pmatrix},$$

when $< y^2 >$, $< yp_y >$, and $< p_y^2 >$ are negligible. The canonical momentum, p_x and p_y can be estimated by using two BPMs with the transfer matrix calculated from the model lattice. The parameter, μ, is obtained from an iterative procedure. The X-Y coupling parameters are obtained by using Eq. 4.14.

Another contribution to the vertical emittance is vertical dispersions. The vertical and horizontal dispersions can be measured by either a rf frequency shift or a rf kick. Skew quadrupole coils at sextupole magnets correct not only the X-Y coupling parameters but also the vertical dispersions. The rotation error of BPMs around the beam axis affects the measurement of both the X-Y coupling parameters and vertical dispersions. However, the optics correction can work and accomplish the requirement if the rotation error of the BPMs is less than 10 mrad.

The beta function is also necessary to correct by either a response of COD or a measurement of phase advance. A feasibility of the optics corrections such as the X-Y coupling, dispersions, and beta functions are studied by computer simulations. Machine error that is assumed in the optics corrections is shown in Table 4.9.

The machine error is estimated from the measurement of the magnet alignment at KEKB. In the simulation, random seeds are generated and the distribution of error is assumed to be a Gaussian distribution. The resolution of BPMs for every measure-

	Δx_{rms} (μm)	Δy_{rms} (μm)	θ_{rms} (mrad)	$(\Delta K/K)_{rms}$
Main dipole	-	-	0.1	3.5×10^{-4}
Quadrupole	100	100	0.1	7×10^{-4}
Sextupole	100	100	-	1.3×10^{-3}
QC1 and QC2	100	100	-	-
BPM	75	75	1	-

Table 4.9: Assumption of machine error for simulations.

	LER	HER	Max. magnetic field
Dipole corrector (H)	218	208	$\theta = 1$ (mrad)
Dipole corrector (V)	196	215	$\theta = 1$ (mrad)
Backleg dipole corrector (H)	33	39	$\theta = 0.5$ (mrad)
Quadrupole corrector coil	292	254	$\Delta K_1/K_1$=0.5 (%)
Skew quadrupole coil*	108 (64)	108 (56)	$K_1 = 5 \times 10^{-3}$ (1/m) for SD,SL

Table 4.10: Number of corrector magnets and coils. H and V indicate horizontal and vertical direction, respectively. *The maximum field of the skew quadrupole coil at SF type is 3×10^{-3} 1/m. Number in parenthesis is the minimum number that includes SD, SL, and/or rotatable SF type at the beginning of the machine operation.

ment is assumed to be 2 μm for the averaged-mode (COD measurement) and 100 μm for the single-pass BPM. The offset of BPMs as shown in Table 4.9 is assumed by a beam-based measurement. The rotation error of BPMs around the beam axis is estimated from manufacture error. The optics corrections include corrections of COD, X-Y couplings, dispersions, and beta functions. The corrector magnets used in the optics correction are shown in Table 4.10. Figure 4.17 shows the vertical emittance after optics measurements by a closed orbit response and corrections. The vertical emittance is corrected to be a few pm by applying the optics corrections while the vertical emittance for the ideal lattice is 0.8 pm in the LER and 1.5 pm in the HER[16]. The optics correction based on the single-pass BPMs is similar to the result of the closed orbit response. The maximum field of $K_1 = 5 \times 10^{-3}$ 1/m for the skew quadrupole coil at the sextupole (SD and SL) is necessary to correct X-Y couplings and vertical dispersions. The closed orbit distortion is corrected by dipole corrector magnets and the vertical angle at main dipole magnets is typically less than 50 μrad. Consequently, synchrotron radiation from the orbit hits within the proper part in the ante-chamber in the LER.

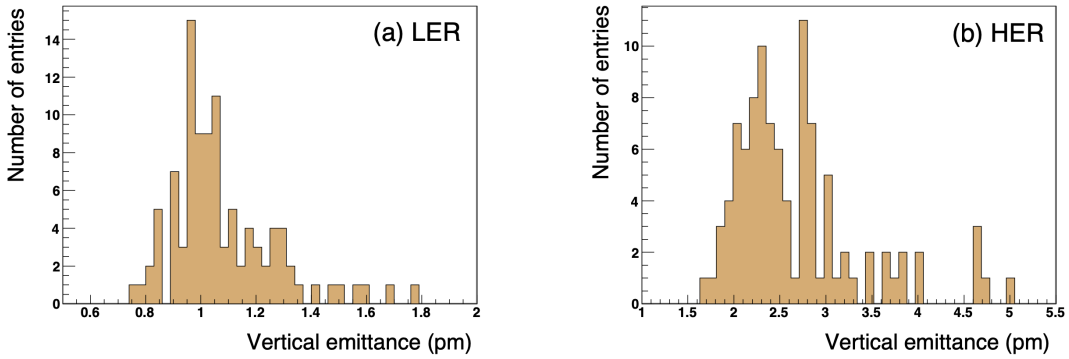

Figure 4.17: Vertical emittance after applying optics corrections is obtained from simulations of 100 samples. (a) LER, (b) HER.

Dynamic aperture after the optics correction is shown in Fig. 4.18. The dynamic aperture for a particle without a momentum deviation is almost recovered by the optics correction. However, the dynamic aperture with momentum deviations decreases compared with the ideal lattice even though the optics correction. It is necessary to correct the off-momentum optics in order to recover the dynamic aperture. The optical parameters, a chromatic phase advance and a chromatic X-Y coupling are expected to be useful to accomplish this purpose. The chromatic phase advance is adjusted by using sextupole magnets and the chromatic X-Y coupling is adjusted by skew sextupole magnets.

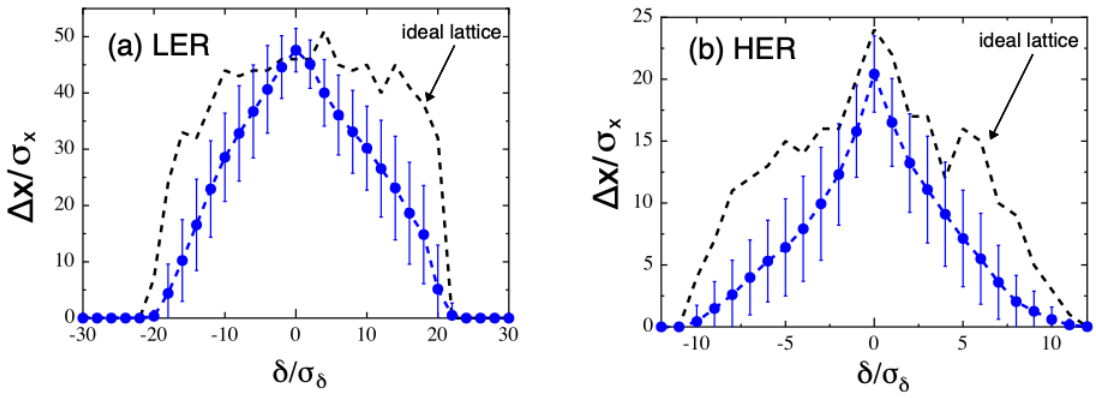

Figure 4.18: Dynamic aperture is an average value (blue plots) obtained from simulations of 100 samples. (a) LER, (b) HER. Bar indicates standard deviation for each momentum deviation. Dashed line indicates dynamic aperture in the ideal lattice.

Horizontal beam position can be measured by using two single-pass BPMs with consecutive turns in the laboratory coordinate system.

$$x_1(n) = \sqrt{2J\beta_1}\cos\psi(n) \tag{4.15}$$

$$x_2(n) = \sqrt{2J\beta_2}\cos\{\psi(n)+\psi_{21}\}, \tag{4.16}$$

where n is the turn number, J is the action variable, β is the beta function at BPMs, and ψ_{21} is the phase advance between two BPMs. The average values of x_1^2, x_2^2, and x_1x_2 can be written by

$$< x_1^2 > = J\beta_1 \tag{4.17}$$
$$< x_2^2 > = J\beta_2 \tag{4.18}$$
$$< x_1x_2 > = J\sqrt{\beta_1\beta_2}\cos\psi_{21} \tag{4.19}$$
$$\tag{4.20}$$

The phase advance, ψ_{21} is obtained by

$$\psi_{21} = \cos^{-1}\frac{< x_1x_2 >}{\sqrt{< x_1^2 >< x_2^2 >}}, \tag{4.21}$$

where the ambiguity of ψ_{21} and $2\pi-\psi_{21}$ remains. Then, the phase advance is measured by changing momentum of particles with shifting a rf frequency. The chromatic phase advance is defined by

$$\frac{\partial\psi_{21}}{\partial\delta}, \tag{4.22}$$

where $\delta = \Delta p/p_0$ is the momentum deviation. The chromatic phase advance in the vertical direction is similar to the horizontal direction. The chromatic X-Y coupling parameters are also defined by

$$\left(\frac{\partial r_1}{\partial\delta}, \frac{\partial r_2}{\partial\delta}, \frac{\partial r_3}{\partial\delta}, \frac{\partial r_4}{\partial\delta}\right). \tag{4.23}$$

The chromatic phase advance and the chromatic X-Y coupling parameters are measured in the whole ring, then those parameters are corrected to be those of the ideal lattice. When the sextupole field is adjusted to optimize the chromaticity, the normal and skew quadrupole field is induced due to the offset of the orbit from the center of the sextupole magnet in general. In order to preserve the optical functions except for the chromaticity before the change, quadrupole correctors neighbor of the sextupole magnet and a skew quadrupole corrector at the sextupole magnet should be adjusted properly. In the case of the rotatable sextupole magnet, we have additional variables of a rotation angle around the beam axis and a strength of the sextupole field.

Fabrication error of QC1 and QC2 such as a misalignment of quadrupole coils is assumed as the machine error. The misalignment of four coils in the radial direction induces either sextupole field or skew sextupole field. The radial displacement of

Δr=35 μm in the opposite way between the left and right side gives approximately the sextupole error field of B_3/B_2=0.1 %. The sextupole and skew sextupole field with an opposite sign between the left and the right side of IP decrease the dynamic aperture significantly. Touschek lifetime as a function of sextupole and skew sextupole error field is shown in Fig. 4.19. For instance, the sextupole field error of $B_3/B_2 = 5 \times 10^{-4}$ decreases Touschek lifetime from about 600 sec to 100 sec. In addition, the skew sextupole field should be corrected at the location of the error field so as to recover enough dynamic aperture. Skew sextupole correctors are placed at QC1R and QC2R to correct the skew sextupole error field and sextupole corrector is placed between QC1R and QC2R to correct the sextupole error field. The octupole correctors are replaced with skew sextupole correctors except for QC1RP. Since QC1RP has no iron yoke, there is the space for both the octupole corrector and skew sextupole corrector. The sextupole corrector and skew sextupole corrector in either the right side or the left side can correct error fields in principle.

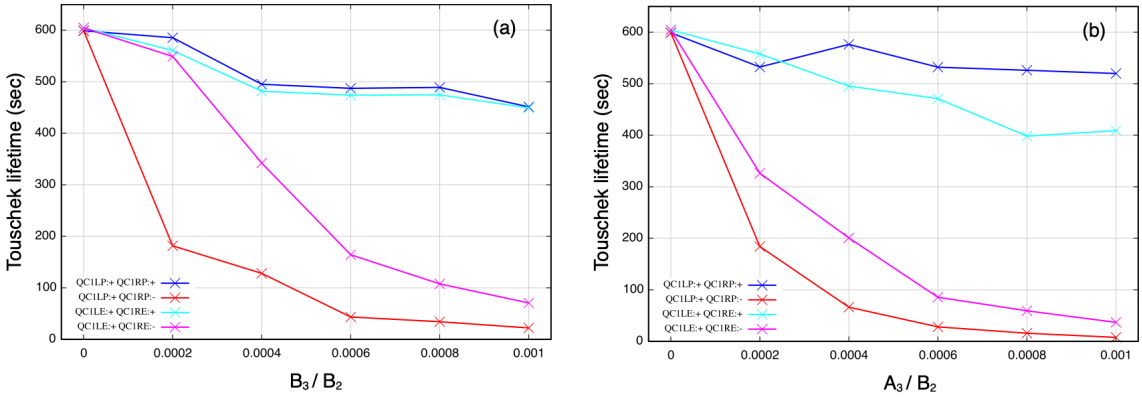

Figure 4.19: Touschek lifetime in the LER and the HER depends on (a) sextupole field error, (b) skew sextupole field error in the QC1s.

4.7 Dynamic Aperture under influence of Beam-Beam Effect

The dynamic aperture is reduced under the influence of a beam-beam effect. Figure 4.20 shows a schematic view of a colliding particle with a large horizontal amplitude. The particle with a horizontal amplitude collides at a location different from IP in the longitudinal direction since two beam lines have the crossing angle of 83 mrad in the

horizontal plane. The deviation along the beam axis is written by

$$\Delta z = \frac{\Delta x}{2\phi_x}, \tag{4.24}$$

where Δx is the horizontal amplitude and ϕ_x is the half crossing angle. The vertical beta function is written by a function of the distance from IP

$$\beta_y(\Delta z) = \beta_y^* + \frac{\Delta z^2}{\beta_y^*}. \tag{4.25}$$

Therefore, the particle with a horizontal amplitude is kicked at a large vertical beta function and the vertical amplitude increases due to the beam-beam interactions if the initial vertical amplitude is non-zero. The vertical amplitude given by the beam-beam kick is

$$\Delta y \propto \theta_y^{bb} \sqrt{\beta_y(\Delta z)}. \tag{4.26}$$

The particle is lost if the vertical amplitude increases and is out of the stable region. In the case of a particle with the horizontal amplitude of $30\sigma_x$ in the LER, the deviation from IP becomes 3.6 mm in the longitudinal direction where the vertical beta function is 48 mm. The vertical beta function becomes 180 times of the nominal beta function at IP.

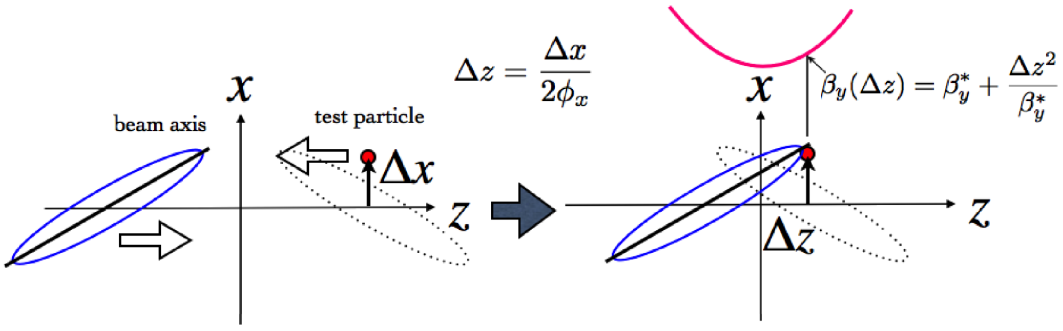

Figure 4.20: Schematic view of collision for a particle with horizontal amplitude in the head-on frame (Weak-Strong model).

Touschek lifetime in the HER reduces about 10 % due to the beam-beam effect, however the impact in the LER is much larger than the HER. Figure 4.21 shows the dynamic aperture in the LER under the influence of beam-beam interactions. The dynamic aperture is reduced significantly compared with that without the beam-beam effect. Especially, the transverse aperture decreases. The white color indicates a stable

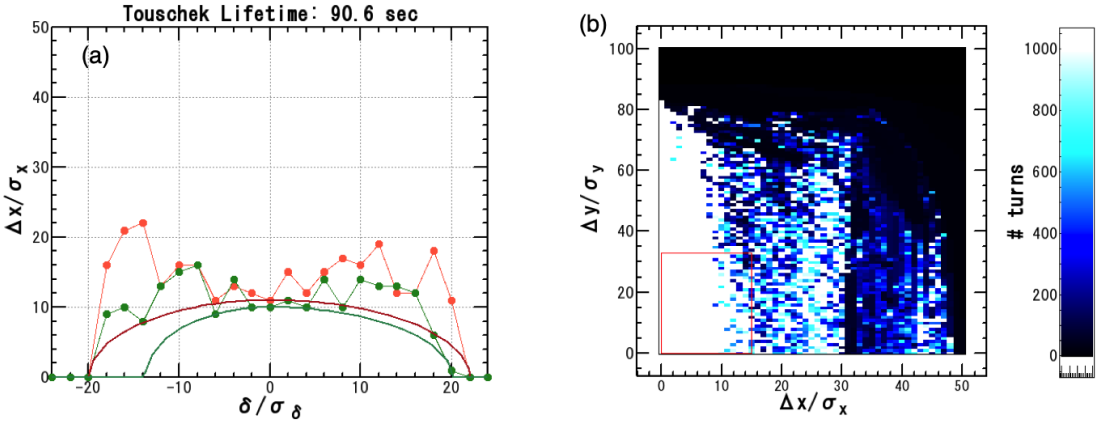

Figure 4.21: Dynamic aperture under the influence of beam-beam effect in the LER. (a) Dynamic aperture in a plane of the horizontal direction and momentum deviation. Ratio of the vertical amplitude to the horizontal is fixed to be nominal emittance ratio as an initial condition. (b) Dynamic aperture in the vertical and horizontal plane. Initial momentum deviation is zero. Red square indicates a requirement for an injection aperture.

region in which the number of turns is larger than 1000 turns. The particle with the horizontal amplitude larger than $10\sigma_x$ is finally lost due to the vertical oscillation even though the vertical initial amplitude is zero because the vertical amplitude is induced by X-Y couplings originate from IR.

Technique of frequency analysis map (FMA)[18] is adopted to understand the chaotic behaviour of the beam-beam interaction[17]. FMA can apply to Hamiltonian system or symplectic map. Therefore, FMA is used to study the motion of the single particle in a storage ring in the world. The results of FMA in the LER are shown in Fig. 4.22. The FMA analysis includes the beam-beam effects but synchrotron motion is turned off. A particle is tracked by 2000 turns and betatron tunes are calculated for the first 1000 turns and again for the second 1000 turns. The tune spread is defined by

$$D = \log_{10} \sqrt{(\nu_{x2} - \nu_{x1})^2 + (\nu_{y2} - \nu_{y1})^2}, \tag{4.27}$$

where (ν_{x1}, ν_{y1}) is obtained from the first 1000 turns and (ν_{x2}, ν_{y2}) from the second 1000 turns. Figure 4.23 shows Poincare plots in the LER. It is found that the 5-th order resonance seems to be induced as increasing a number of particles in the HER (strong beam).

Scan of the dynamic aperture with the beam-beam effect in the betatron tunes is performed in the LER as shown in Fig. 4.24 (a). The momentum deviation and

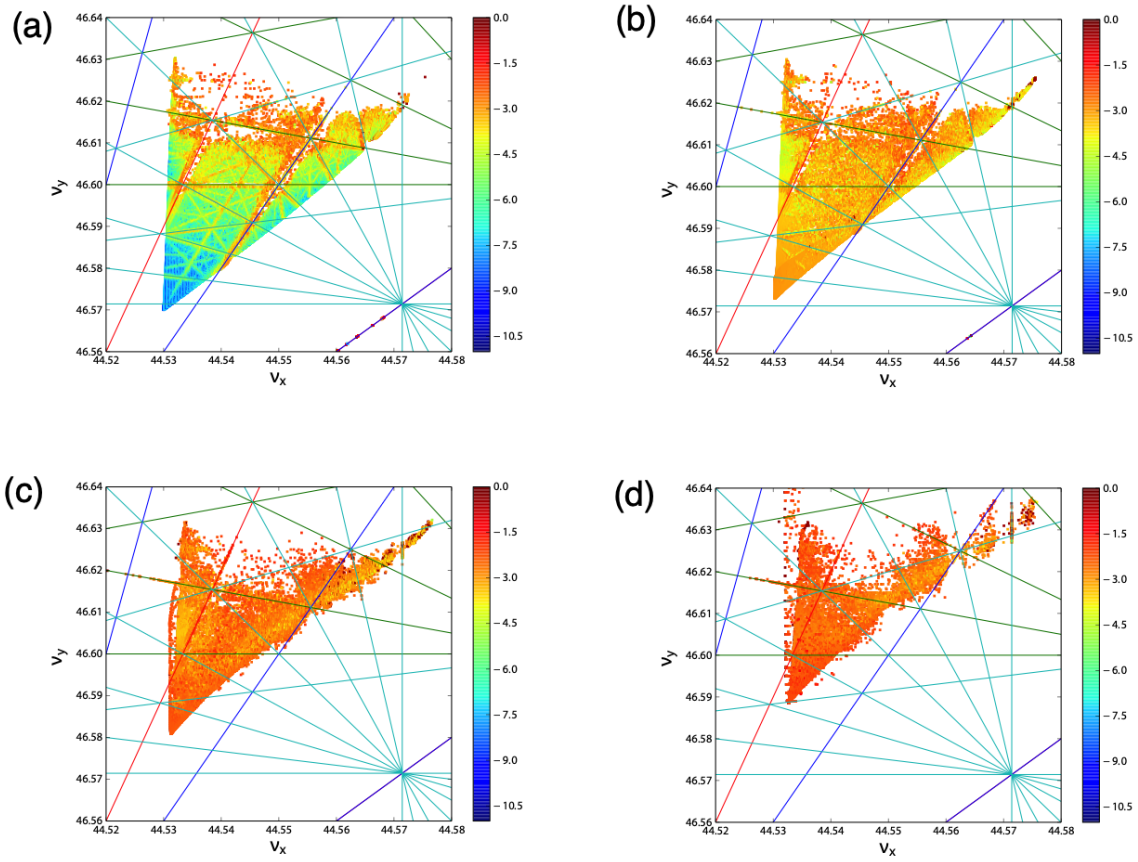

Figure 4.22: Results of FMA in the LER. (a) No beam-beam, (b) 10 %, (c) 50 %, (d) 100 % of nominal colliding particles. The color indicates a rate of tune spread described in the text. Red line indicates 4-th order resonance, green indicates 5-th order, blue indicates 6-th order, and cyan indicates 7-th order.

the vertical amplitude are zero as the initial condition. There is a better working point near the half integer resonance in the vertical direction. However, the chromaticity correction becomes difficult near the half integer resonance. Consequently, the dynamic aperture for off-momentum particles decrease and then Touschek lifetime becomes short. Another candidate for the working point is near X-Y coupling resonance in the betatron tune scan. Figure 4.24 (b) shows the dynamic aperture with the beam-beam effect for the working point of $(\nu_x, \nu_y) = (44.53, 46.54)$. Touschek lifetime is improved to be 231 sec, however it is not enough lifetime for the beam operation.

The another approach to compensate the beam-beam kick for the large horizontal amplitude is a crab-waist scheme. Hamiltonian of the crab-waist term is

$$H_{CW} = \frac{\lambda}{2} x p_y^2, \tag{4.28}$$

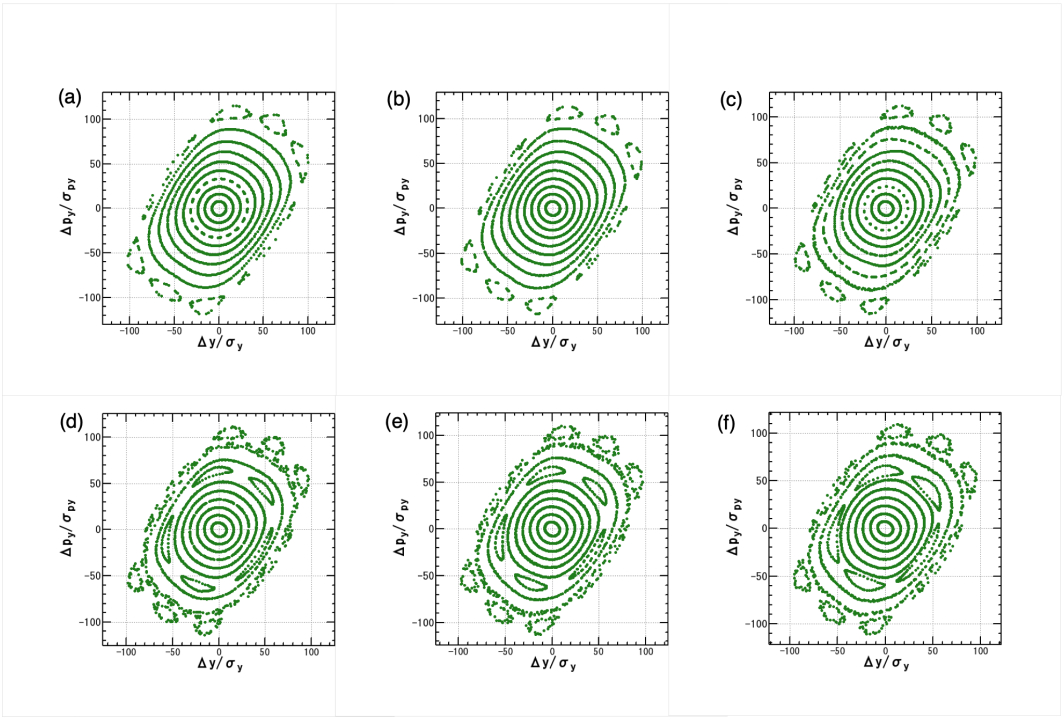

Figure 4.23: Poincare plots in the vertical direction in the LER. Poincare plot depends on number of particles of a strong beam. Nominal number of particles per bunch is 6.53×10^{10} in the HER (strong beam). (a) 0 %, (b) 20 %, (c) 40 %, (d) 60 %, (e) 80 %, (f) 100 %.

where

$$\lambda = \frac{1}{\tan 2\phi_x}. \tag{4.29}$$

If we consider the ideal case of the crab-waist scheme, the map of the beam-beam interaction is replaced with

$$f_{BB} \to f_{CW}(+\lambda) \cdot f_{BB} \cdot f_{CW}(-\lambda), \tag{4.30}$$

where the map of the crab-waist is

$$f_{CW}(\lambda) : p_x \quad \to \quad p_x + \frac{\lambda}{2} p_y^2 \tag{4.31}$$

$$y \quad \to \quad y - \lambda x p_y. \tag{4.32}$$

The feasibility of the ideal crab-waist is studied by using tracking simulations and the dynamic aperture in the transverse plane is shown in Fig. 4.25 (b). The dynamic aperture is almost recovered by the ideal crab-waist that is compared with Fig. 4.21. Sextupole magnets are utilized to accomplish the crab-waist in the realistic lattice as

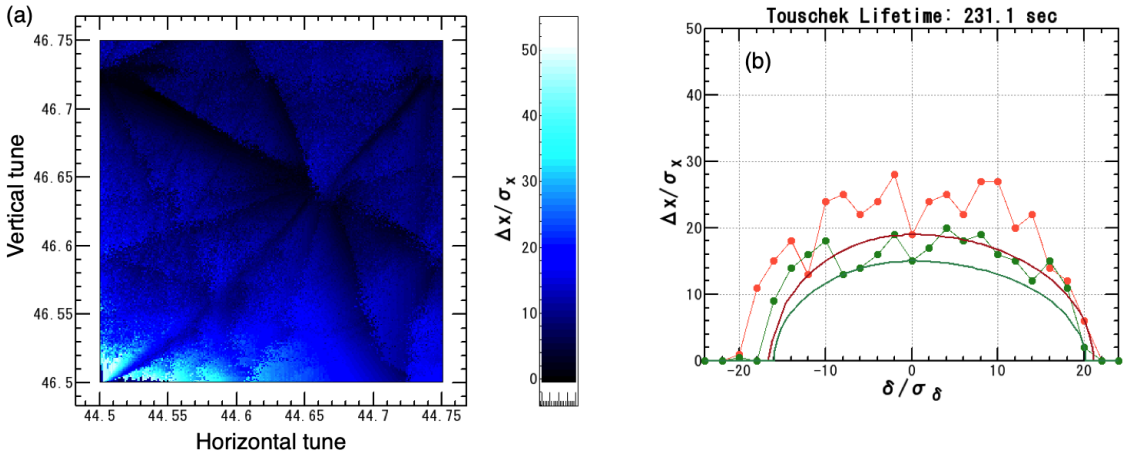

Figure 4.24: Dynamic aperture under the influence of beam-beam effect in the LER. (a) Dynamic aperture without a momentum deviation in the plane of betatron tunes. (b) Dynamic aperture for $(\nu_x, \nu_y) = (44.53, 46.54)$. The optimization of sextupoles and octupoles are applied. Ratio of the vertical to the horizontal amplitude is fixed to be the nominal emittance ratio.

described the Sect. 4.8. In the case of sextupole magnets, the x^3 term is added to the crab-waist term in the Hamiltonian, however, it can be almost ignored by choosing a large ratio of the horizontal beta function to the vertical at the sextupole magnets.

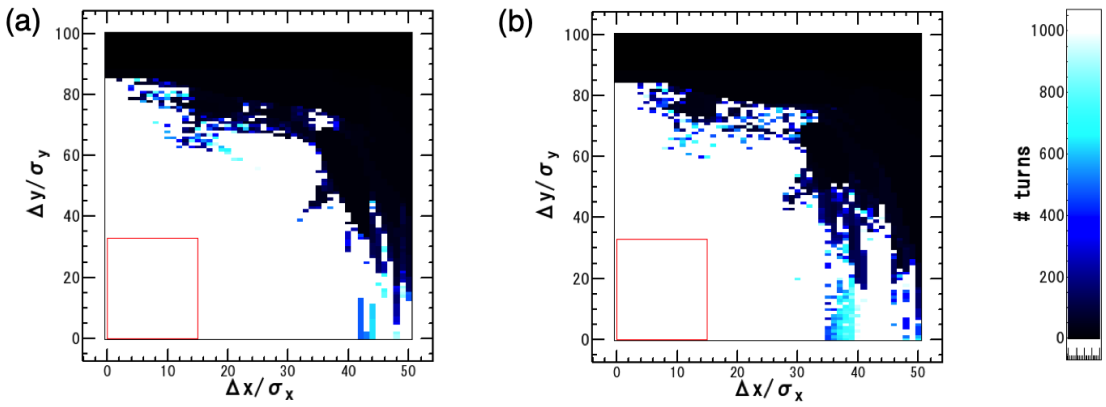

Figure 4.25: Dynamic aperture in the LER, (a) without beam-beam effect, (b) with the ideal crab-waist under the influence of beam-beam effect. The initial vertical amplitude and momentum deviation are zero. Red square indicates a requirement for an injection aperture.

4.8 Crab-Waist Scheme

The dynamic aperture under the influence of the beam-beam effect decreases significantly. An hourglass effect is an issue for a larger horizontal amplitude of a particle that affects the dynamic aperture even though the low emittance is adopted. In order to overcome the difficulty in the colliding beams, a cure of *crab-waist scheme* is considered. The crab-waist scheme is proposed by P. Raimondi et al. for the SuperB project[1]. The crab-waist scheme can reduce the hourglass effect together with the nano-beam scheme. In the crab-waist scheme, two sextupole magnets are placed for each side of IP and shift a waist of colliding particles having a horizontal amplitude to cancel the deviation from the waist. The betatron phase advance between a crab-waist sextupole magnet and IP is adjusted to be $m\pi$ in the horizontal direction and $(n+1/2)\pi$ in the vertical direction, where m and n are arbitrary integers. The strength of the crab-waist sextupole is

$$\mid K_2 \mid = \frac{1}{\tan 2\phi_x \beta_y^* \beta_{y,s}} \sqrt{\frac{\beta_x^*}{\beta_{x,s}}}, \tag{4.33}$$

where $\beta_{x,s}$ and $\beta_{y,s}$ are the horizontal and vertical beta function at the crab-waist sextupole, respectively. The sign of K_2 is chosen so as to shift the waist at IP properly and cancel a nonlinear kick between a pair of crab-waist sextupole magnets. A candidate of the location of crab-waist sextupoles is the OHO and NIKKO straight section since there is no dispersion and the chromaticity correction is not affected for the reference particle. The lattice design for the crab-waist scheme in the LER is shown in Fig. 4.26. The crab-waist sextupole is assumed to be a thin lens for the study in this report. The machine parameters for the crab-waist scheme in the LER are shown in Table 4.11.

	Symbol	LER	Unit
Horizontal beta at IP	β_x^*	32	mm
Vertical beta at IP	β_y^*	270	μm
Half crossing angle	ϕ_x	41.5	mrad
Horizontal beta at CW sextupole	$\beta_{x,s}$	8.5	m
Vertical beta at CW sextupole	$\beta_{y,s}$	200	m
Horizontal phase advance between IP and CW sextupole	$\Delta\psi_x$	25π	rad
Vertical phase advance between IP and CW sextupole	$\Delta\psi_y$	26.5π	rad
Nominal field of CW sextupole	$\mid K_2 \mid$	13.66	$1/m^2$

Table 4.11: Machine parameters for the crab-waist scheme in the LER.

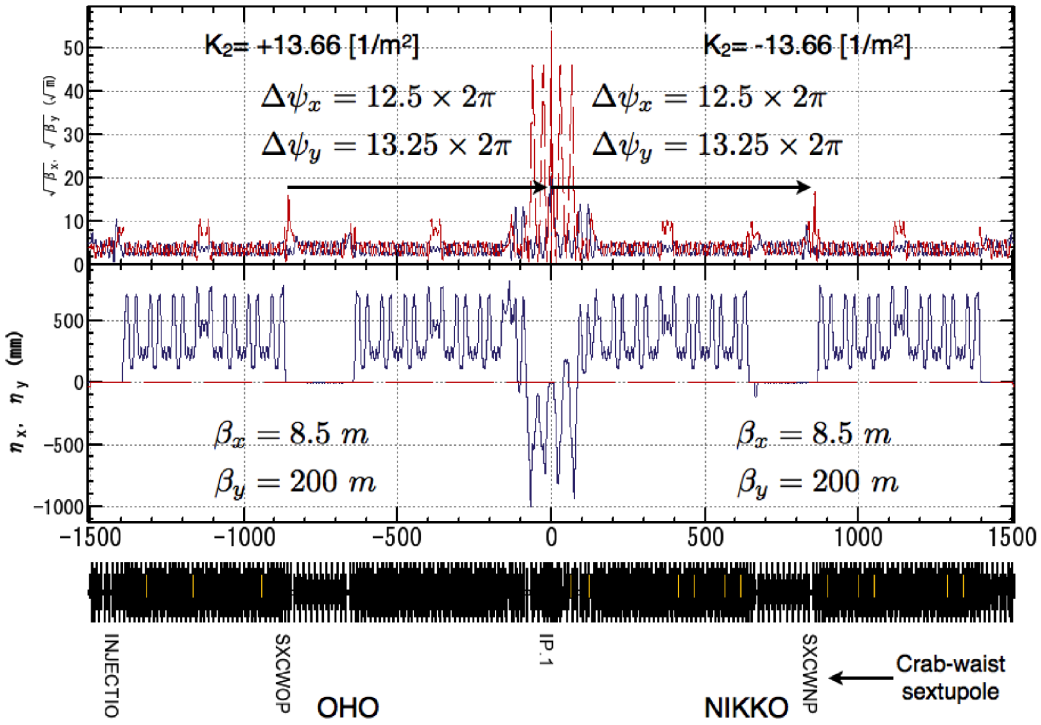

Figure 4.26: Lattice design for the crab-waist scheme in the LER.

Figure 4.27 shows transverse dynamic apertures in the LER as a function of K_2 for the crab-waist sextupoles. The initial momentum deviation is zero in the simulations. The dynamic aperture decreases as increasing the field strength of the sextupoles even though the beam-beam interaction is turned off as shown in Figs. 4.27 (a) and (b). The nonlinear kick due to the crab-waist sextupole for the reference particle can be canceled by another sextupole, however, it cannot be canceled for a particle with a large amplitude. The term of $\Delta p_y = K_2 xy$ increases the vertical amplitude of the particle, then the particle is lost and the dynamic aperture is reduced. The dynamic aperture is reduced even though the initial vertical amplitude is zero since the vertical oscillation for the large horizontal amplitude is induced by the X-Y coupling which depends on the amplitude of the oscillation. Figures 4.27 (c) and (d) show the dynamic aperture under influence the beam-beam interaction. The dynamic aperture is recovered by the crab-waist sextupoles as increasing the field strength until the nonlinear kick from the sextupoles restricts the aperture. Therefore, it implies the difficulty comes from the cancellation of the nonlinear kick by a pair of crab-waist sextupoles for the large amplitude of a particle without the beam-beam effect. The dynamic aperture without the beam-beam effect in the crab-waist optics is shown in Fig. 4.28. If the crab-waist sextupoles are turned on with 80 % of the nominal field strength, Touschek

lifetime becomes 74 sec. Both of the transverse and momentum aperture are reduced significantly. The solution to recover the dynamic aperture has not been found by optimizing the conventional sextupoles and octupoles so far.

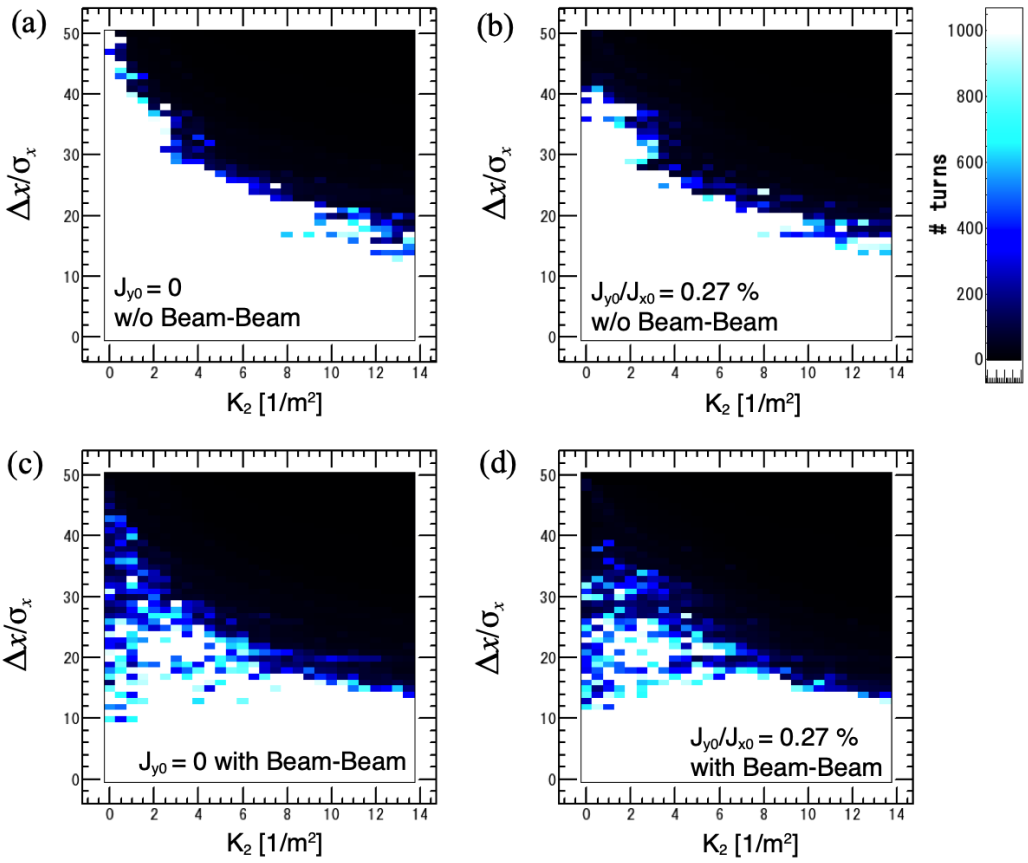

Figure 4.27: Transverse dynamic aperture as a function of K_2 for crab-waist sextupoles in the LER. (a) Initial vertical amplitude is zero without beam-beam effect. (b) Ratio of the vertical to the horizontal amplitude is 0.27 % as an initial condition. Beam-beam effect is turned off. (c) Initial vertical amplitude is zero with beam-beam effect. (d) Ratio of the vertical to the horizontal amplitude is 0.27 % as an initial condition. Beam-beam effect is turned on.

In order to investigate the reduction of the dynamic aperture in the crab-waist scheme, a simple model for the IR lattice is considered in the LER as an ideal case. The IR model is simplified to be no solenoid field, no offset of the final focus quadrupole magnets, and no higher-order multipole fields from IP (s=0) to s=4 m for each side of IP. The transverse dynamic aperture for the on-momentum particle as a function of K_2 of the crab-waist sextupoles is shown in 4.29. The dynamic aperture becomes slightly larger than the nominal IR model at the nominal field of the sextupoles, however, the

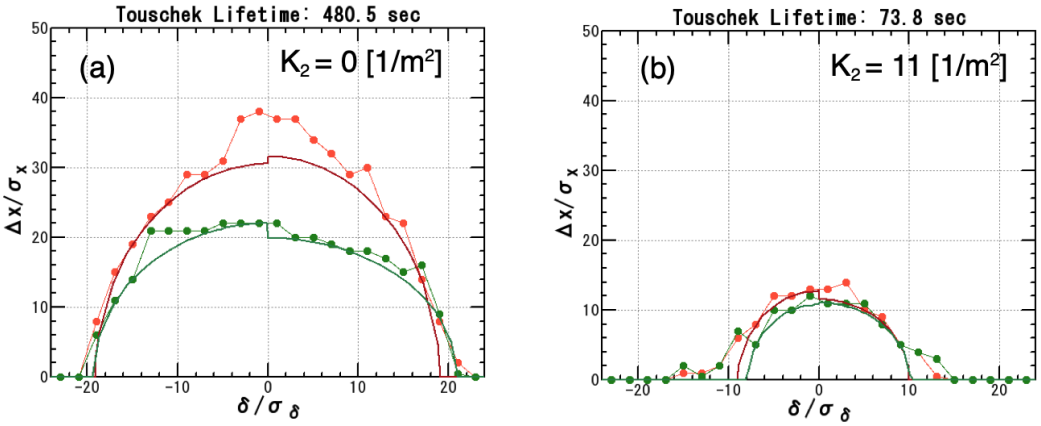

Figure 4.28: Dynamic aperture in the LER crab-waist lattice without beam-beam effect. Initial ratio of the vertical to the horizontal amplitude is 0.27 %. (a) $K_2 = 0$ [1/m^2], (b) $K_2 = 11$ [1/m^2].

aperture is about $20\sigma_x$ at most. The dependence of the field strength of the sextupoles to the dynamic aperture still exists. In addition to the simple IR, QC1 and QC2 in which nonlinear Maxwellian fringe fields are turned off are considered to study the dynamic aperture. The transverse dynamic aperture as a function of K_2 of the crab-waist sextupoles is shown in Fig. 4.30. The dependence of the field strength is almost disappeared for the dynamic aperture. The dynamic aperture is recovered by using the crab-waist sextupoles under the influence of the beam-beam interaction. Therefore, the issue is how to linearize the lattice between two sextupoles that include the nonlinear IR in the realistic lattice.

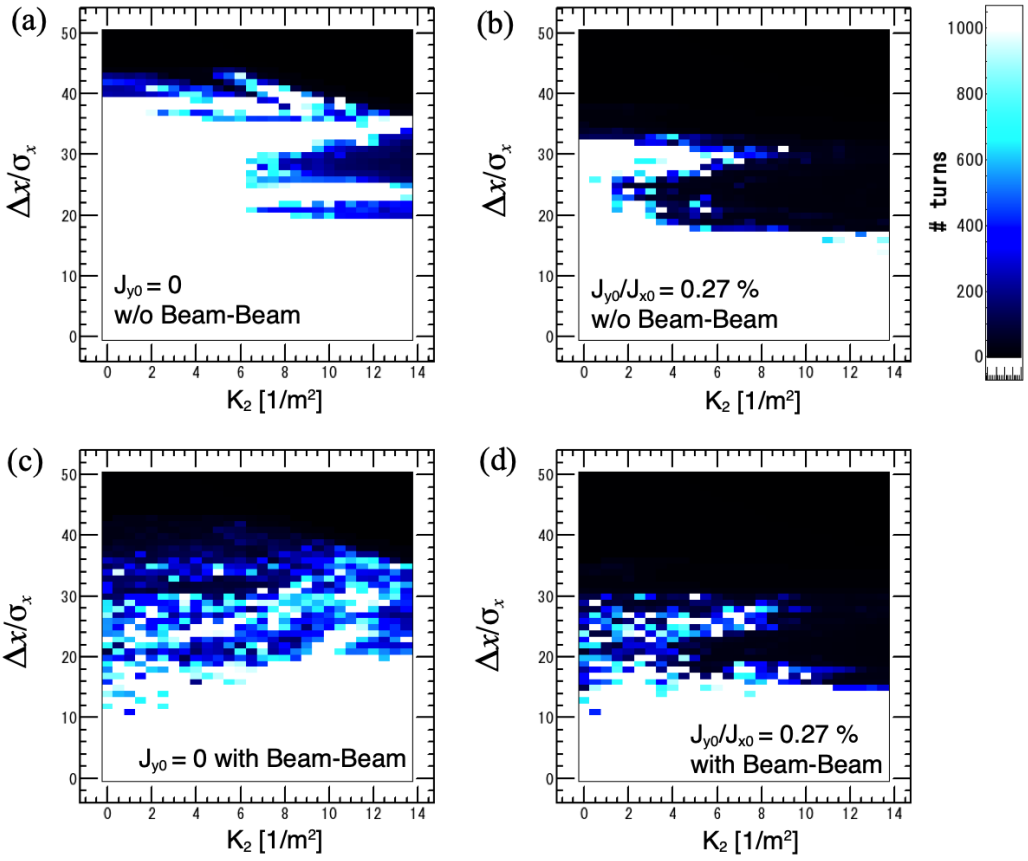

Figure 4.29: Similar figures to Fig. 4.27 for simple IR lattice.

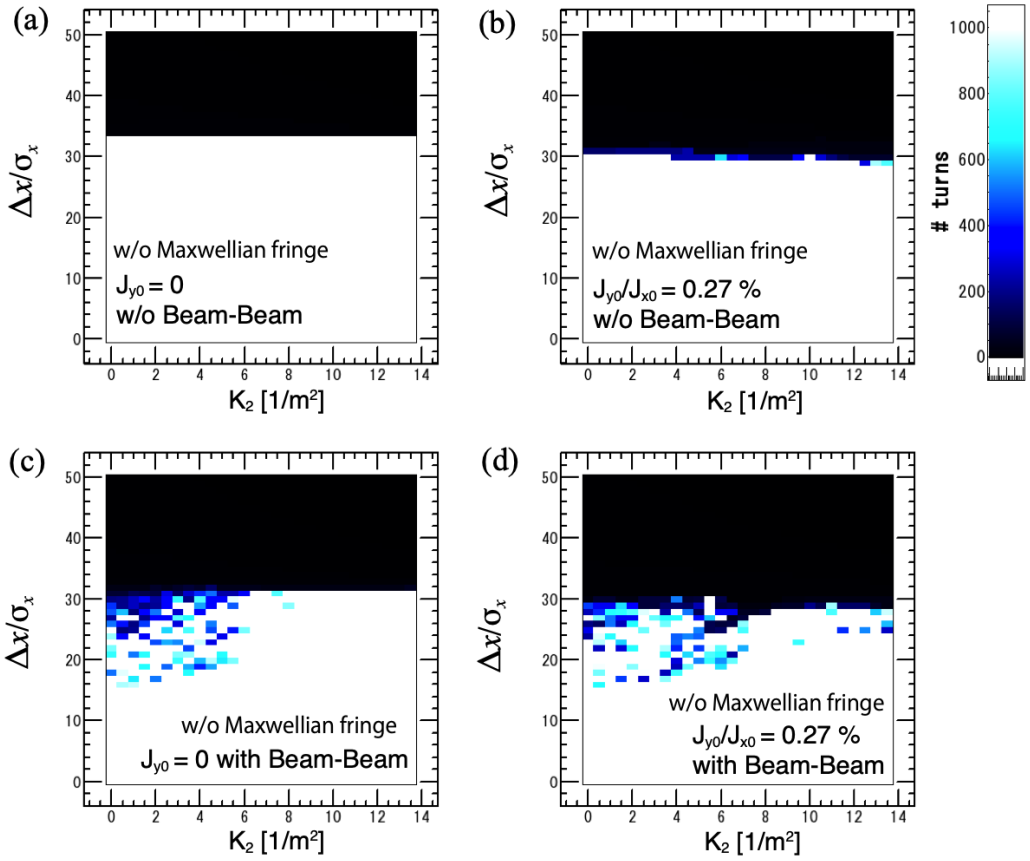

Figure 4.30: Similar figures to Fig. 4.27 for simple IR lattice. In addition, nonlinear Maxwellian fringe fields in the QC1s and QC2s are turned off.

Bibliography

[1] "SuperB Conceptual Design Report", INFN/AE-07/2, SLAC-R-856, LAL 07-15, March 2007.

[2] KEKB B-Factory Design Report, KEK Report 95-7 (1995).

[3] KEKB Accelerator Papers, KEK Preprint 2001-157 (2001).

[4] A. Piwinski, in Proc. of the 9th International Conference on High Energy Accelerators, Stanford, (1974) 405.

[5] J. Bjorken and S. Mitingwa, Part. Accel. **13**, (1983) 115, FERMILAB-Pub-82/47-THY July, 1982.

[6] K. Kubo and K. Oide, Phys. Rev. ST Accel. Beams **4**, 124401 (2001).

[7] *Strategic Accelerator Design*, http://acc-physics.kek.jp/SAD.

[8] R. H. Helm et al., IEEE Trans. Nucl. Sci. **20** (1973) 900-901.

[9] K. Ohmi, K. Hirata, and K. Oide, Phys. Rev. **E49** (1994) 751-765.

[10] K. Oide and H. Koiso, Phys. Rev. **E47** (1993) 2010-2018.

[11] A. Morita et al., Proc. of IPAC'11, THPZ005, September 2011.
A. Motita et al., Proc. of IPAC'12, TUPPC018, May 2012.

[12] http://www.ansys.com.

[13] H. Yamaoka et al., Proc. of IPAC'12, THPPD023, May 2012.

[14] M. Masuzawa and R. Sugahara, KEK-PREPRINT-2003-97 (2003).

[15] Y. Ohnishi et al., Phys. Rev. ST Accel. Beams **3** 091002 (2009).

[16] H. Sugimoto et al., Proc. of IPAC'12, TUPPC020, May 2012.

[17] D. Zhou et al., Proc. of IPAC'12, TUPME016, May 2012.

[18] D. Shatilov et al., Phys. Rev. ST Accel. Beams **14**, 014001 (2011).